Resolving cross-shelf dynamics in the Agulhas Current from GlobCurrent and glider observations

Author:

Tumelo Maja

Supervisors:

Dr. Marjolaine Krug

Oceanography (HRA), Council for Scientific and Industrial Research (CSIR), Natural Resources and the Environment

Prof. Mathieu Rouault

Department of Oceanography, University of Cape Town (UCT)

Prof. Johnny A. Johannessen

Nansen Environmental and Remote Sensing Center (NERSC), Bergen, and
Geophysical Institute, University of Bergen, Norway

October 2019

Submission made to the Department of Oceanography at the University of Cape Town as a partial academic requirement for fulfilment of Masters (MSc) degree in Applied Ocean Sciences

Abstract

The Agulhas Current is the strongest Western Boundary Current of the Southern Hemisphere and it plays a significant role in the circulation of the shelf and coastal waters, whereby mesoscale (50- 500 km) and submesoscale (1 -10 km) instabilities in the Agulhas Current impact the local oceanography of the shelf region. The main objective of this study is to evaluate the ability of a gap-free and merged gridded satellite ocean current dataset, GlobCurrent, to resolve and monitor the variability of the Agulhas Current's cross-shelf dynamics. In this study, GlobCurrent is compared to in-situ observations collected from underwater gliders through mapping and correlation analysis to assess the product's accuracy in different subdomains and water depths of the Agulhas Current's main area domain. We also investigate the value of using a higher resolution satellite and gap-free Sea Surface Temperature (SST) dataset to complement the GlobCurrent dataset in observing the Agulhas Current's flow processes and features. The results show that GlobCurrent is adequate for describing large mesoscale features and deep water flows but the product has limitations in capturing fast-evolving and small mesoscale features, particularly the Durban Eddy in the KZN bight region. GlobCurrent also exhibits, at times, directional errors in addition to the current speed discrepancies. This research study demonstrates the limitation of the GlobCurrent product for monitoring ocean current variability in shallow, coastal waters and regions dominated by small mesoscale variability. This study also provides new insights on the joint use of other merged satellite products i.e. merged ODYSSEA SST, which may compensate for some of the GlobCurrent product's shortfalls. Future studies should consider complementing altimetry-based satellite products like GlobCurrent with other merged satellite observation products such as ODYSSEA SST for better imaging of small mesoscale processes and features in shallow coastal waters.

Declaration

I, …..**Tumelo Maja**... declare that the content of this thesis is my own unaided work. All contributions from other authors or sources have been acknowledged and referenced. Furthermore, content in this document represents my own opinions and not necessarily those of the University of Cape Town.

Signature: Signed by candidate
……
Date: ……15 November 2019 ..

Tumelo Maja

Acknowledgments

I would like to express sincere gratitude to the following people that were very helpful and supportive in many aspects throughout the year up to the completion of this thesis document:

Firstly and most importantly, I would like to thank God for the strength He has given me to succeed in this academic journey. Secondly, my family for the great support from the beginning of this academic year and throughout. Great thanks to my supervisors, Dr. Marjolaine Krug, Prof. Johnny A. Johannessen, and Prof. Mathieu Rouault, for the guidance and support both financially and academically. Special thanks to Prof. Johnny A. Johannessen and Dr. Anthony Bosse (Geophysical Institute, University of Bergen). All postgraduate students in the UCT oceanography department and those at the NERSC in Norway, notably Abhishek Shah for help with glider data processing and coding skills. All members of the Oceanography department staff who recommended readings and provided technical and academic support. Funding for this MSc degree was provided by the Nansen Tutu Center and the National Research Fund (NRF) both via Prof. Mathieu Rouault SARCHI Chair, the assistance is sincerely acknowledged. Cashifa Karriem for encouragement and support with admin and for refreshing conversations. Thembalethu Shangase for great support and motivation at times of stresses and frustrations, and for emotional and psychological support. All my friends have shown support to me throughout the year.

Table of Contents

List of Figures

List of Tables

CHAPTER 1 – INTRODUCTION

1.1. Background

Western Boundary Currents (WBC's) have strong mean kinetic energy (MKE) and are also associated with high levels of eddy kinetic energy (EKE) (Zhai et al., 2010). Some of the energy contained in the mean WBC jet is dissipated towards the smaller scales with impacts felt in the coastal and shelf regions. The Agulhas Current (AC) is the strongest WBC of the Southern Hemisphere and it plays a significant role in the circulation of shelf and coastal waters, whereby mesoscale (50- 500 km) and submesoscale (1 -10 km) instabilities in the Agulhas Current impact the local oceanography of the shelf region (Krug et al., 2014). Lutjeharms et al. (2003) gives a description of the spatial variability of the Agulhas Current by distinguishing two parts within the current flow domain; the northern and the southern Agulhas Current. In the northern Agulhas Current, where the shelf is steep and narrow, the current is strongly steered by topography and its path is usually stable. Mean Agulhas Current velocities in this region peak at 1.6 m/s (Gründlingh, 1983; Lutjeharms, 2006). Further south, the shelf starts widening south of Port Elizabeth until it reaches its furthest extent from the land around 27°S:21°E (Lutjeharms, 2006). In the southern Agulhas, the widening of the shelf reduces the influence of topographic steering on the current flow. As a result, the Current exhibits a larger variability as it detaches from the narrow shelf following its edge (De Ruijter et al., 1999; Lutjeharms, 2006).

The narrow and intense flow of the Agulhas Current is often perturbed by the passage of mesoscale meanders called Natal Pulses (Rouault and Penven, 2011). These mesoscale meanders can be identified distinctive negative (positive) Sea Level Anomalies (SLA) in the inshore (offshore) edge of the flow (Leber et al., 2017). Previous studies have shown that the generation of Natal pulses is associated with the westward propagation of deep-ocean eddies from the Agulhas Current source regions towards the Agulhas Current jet (Tsugawa and Hasumi, 2010; Braby et al., 2016). While a significant number of Natal Pulses dissipate along the topographic boundary (Rouault and Penven, 2011), some are able to extract kinetic

energy from the Agulhas Current to grow as they propagate downstream (Elipot and Beal 2015).

The Agulhas Current also exhibits fluctuations at the inshore edge driving the submesoscale variability and vorticity generation through barotropic shear instability (Gula et al., 2015 and 2016). Along the downstream flow, submesoscale cyclonic (anticyclonic) eddies are generated on the inshore (offshore) side where the mean flow interacts with topography (Gula et al 2016). The 1st glider observations in the Agulhas Current confirmed that small submesoscale eddies are generated at the inshore edge of the Agulhas Current as a result of shear instability, with the cyclonic eddies extracting their energy from the mean jet flow (Krug et al., 2017). Such cyclonic eddies are part of a range of submesoscale processes that are generated by the interaction of the Agulhas Current with coastal waters and the coastal topography (Lutjeharms, 2006; Krug et al., 2014; Krug et al., 2017). Changes in the Agulhas Current's flow strength or the position of the core flow can modify the hydrographic condition of shelf waters and occasionally lead to a cross and along-shelf exchange of waters (Boyd, 1994; Krug et al., 2014; Pivan et al., 2016; Leber et al., 2017).

Elevated activity of eddies can modify the oceanic condition and biogeochemical flux of nutrients and thus affect biological productivity (Roughan et al., 2011). Monitoring the variability of the Agulhas Current over time also directly benefits all maritime-related industries, for example, providing insight on the advection and dispersion of fish larvae or other water particles such as chemical or natural pollutants from oil spills and toxic algal blooms. Observing and monitoring variability is therefore important for a better understanding of our marine ecosystems and to support marine industries. Scientists and researchers have made use of various tools and techniques to monitor, forecast and study ocean processes in order to gain a better understanding of the ecological, economic and physical services that oceans provide. The use of both in-situ and remotely sensed observations jointly with model simulations has advanced the research capabilities and allowed better insight of upper ocean dynamics and interactive processes across a broad

range of spatial and temporal scales (Roberts et al., 2016; Rouault and Penven 2011; Guastella and Roberts, 2016; Tsugawa and Hasumi, 2010; Hart-Davis et al. 2018).

1.2. Motivation for the Study

While *in-situ* and satellite observations provide highly important data for studying ocean flow processes, it is necessary to know how accurately satellite products can represent ocean processes. Once the limitations and capabilities of satellite products are established, they can be used to extend the study of various processes to regions without *in-situ* observations to look at ocean variability over larger temporal and spatial scales.

1.3. Research Objectives

The main objective of this study is to evaluate the ability of a gap-free and merged satellite ocean current dataset, GlobCurrent, to resolve and monitor the variability of the Agulhas Current's cross-shelf dynamics. In this study, GlobCurrent is compared to in-situ observations collected from underwater gliders. The ability of the merged product to reproduce the Agulhas Current frontal variability at both meso and submesoscales is assessed. It is hoped that our findings will inform users of the limitations of merged current satellite products in the region and will also guide future developments for such products.

1.4. Research Questions

- What is the accuracy of GlobCurrent product in the Agulhas Current region?
- Can GlobCurrent adequately capture mesoscale variability?
- Is the performance of GlobCurrent region dependent?
- Would other merged products such as ODYSSEA SST be more suited to track the Agulhas Current variability over the shelf regions?

1.5. Outline of the Thesis

The thesis contains 6 chapters. Chapter 1 introduces the research background, the motivation for the study and the research questions and objectives. Chapter 2 presents a literature review on the Agulhas Current, the Shelf Circulation over the Agulhas Bank, Mesoscale processes focusing on dominant circulation features in the Agulhas Current and lastly submesoscale processes. Chapter 3 describes the *in-situ* glider and satellite datasets and methodologies used to process the data. We present our results in Chapter 4. A discussion of the results is made in Chapter 5. Chapter 6 summarises the main findings and provides some recommendations for future research studies in the field.

CHAPTER 2 – LITERATURE REVIEW

2.1 The Agulhas Current

The Agulhas Current flows adjacent to the Eastern South African coast in a south-westward direction (figure 2.1.1). The Agulhas Current forms part of a large subtropical gyre in the south Indian ocean which includes the Retroflection region and the Return Current (Stramma and Lutjeharms 1997). The upstream flow of the Agulhas starts approximately at 27°S on the east coast of South Africa (Lutjeharms, 2006). In this region, the Mozambique basin with the observed high frequency of eddy activity feeds water into the Agulhas Current (Halo et al., 2014). Eddies originating from the South-East Madagascar Current and the Mozambique Channel are important sources of water flow for the Agulhas Current (Halo et al., 2014; Backeberg et al., 2008). In the south-east of South Africa (from 34°S), along the eastern Agulhas Bank (south of 34°S – 36.5°S) the Current veers away from the coast. The Agulhas Current then turns predominantly westward, sometimes in a meandering pattern (Duncombe Rae, 1991). At around 40°S and 18-20°E, a large proportion of the Agulhas Current flow retroflects and switches from a south-westward flow to a predominantly eastward flow as the Return Current (Duncombe Rae, 1991). This area, known as the Retroflection is characterized by the highest mesoscale variability worldwide (Garzoli et al., 1996). The dominant mode of variability at the Retroflection is associated with the shedding of anticyclonic eddies that transport warm and saline waters from the Indian Ocean to the Atlantic Ocean (Lutjeharms and van Ballegooyen, 1988). These anticyclonic eddies, termed Agulhas rings, are the main contributor to the Indian- Atlantic inter-oceanic exchange, termed Agulhas Leakage (Van Leeuwen et al., 2000; Backeberg et al., 2008). Occasionally, changes in the path of the Agulhas Current can trigger an early Retroflection (Krug and Tournadre, 2012).

Beal at al. (2015) estimated the Agulhas Current to have a width of 219 km and a maximum depth of 3000 m. With averaged surface current speeds reaching 1.8 $m.s^{-1}$, the mean flow has a transport of about -84 Sv ($1\ Sv = 10^6 m^3 s^{-1}$). A weak northerly flow, the Agulhas

Undercurrent, has been observed at depths below 1200 m on the continental slope (Beal at al., 2015). The Agulhas Current current core is manifested as the area of highest SSH gradient, maximum ocean current velocity and highest SST, warmer than surrounding waters (Lutjeharms, 2006; Krug and Tournadre 2012). From the shoreward boundary of the Current, the alongshore current increases rapidly and peaks at the core, followed by a gradual drop towards the offshore boundary (Lutjeharms, 2006; Krug and Tournadre 2012). Using along-track altimetry, the Agulhas Current has been shown to display abrupt changes in velocities and direction (Krug and Tournadre 2012).

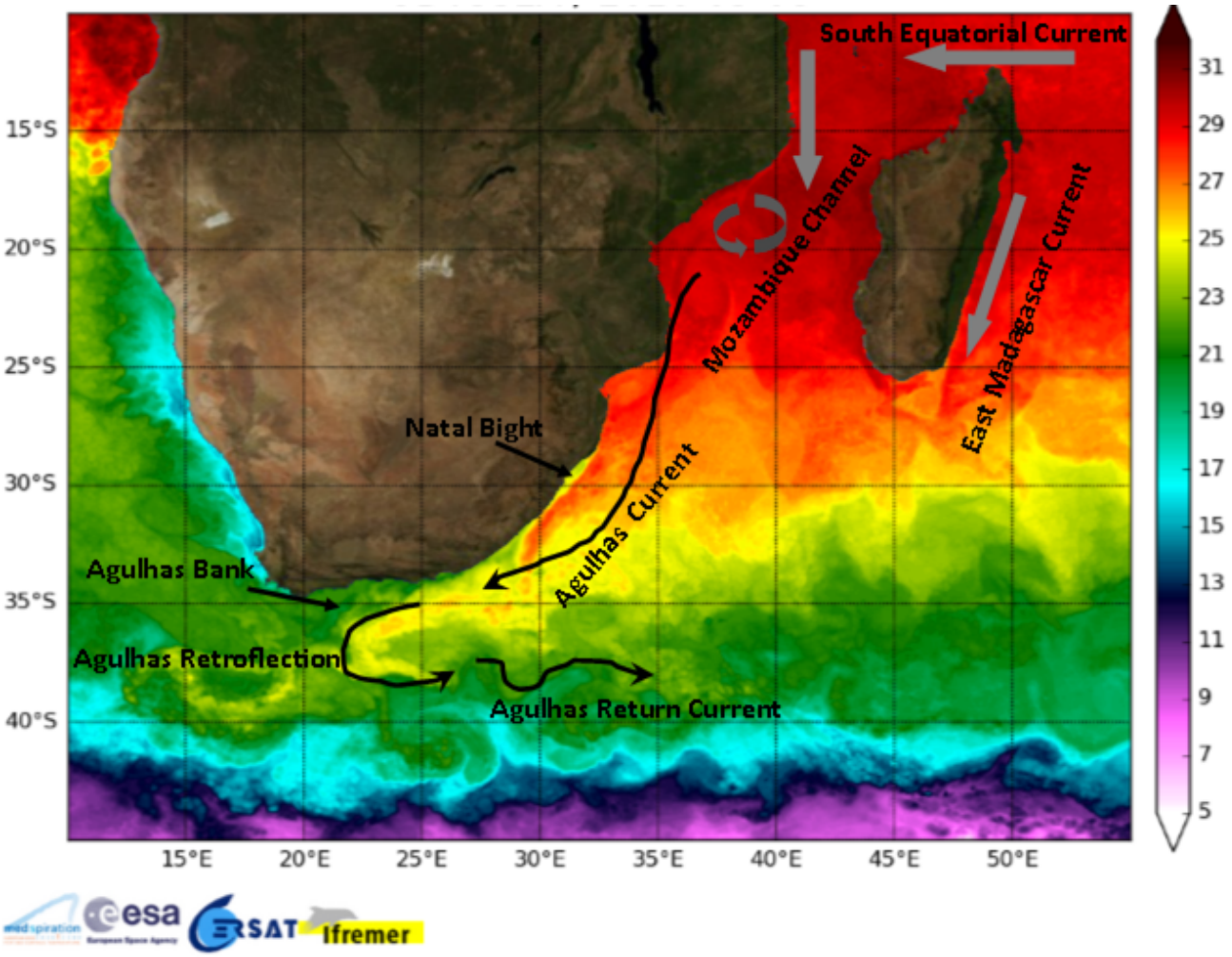

Figure 2.2.1:Map of Sea Surface Temperature fields of the Southern African coastlines showing the greater Agulhas Current system on 08/03/2016. The colour bar indicates the SST values corresponding to the colours on the map (adapted from ODYSSEA South-Africa SST Analysis, source: http://cersat.ifremer.fr/thematic-portals/projects/medspiration/visualization/quicklooks/south-africa).

During meandering, the passing of cyclonic and anticyclonic circulation anomalies induce upwelling (downwelling) on the leading (trailing) edge of the Current meander (Campos et

al. 2000; Pivan et al., 2016). In the northern region of the Agulhas Current where both the shelf and slope are narrow, the intense core of the flow inhibits the mixing as it is closest to the coast (i.e. 20 km) and consequently the upwelling events have been thought to have lower frequency of occurrence (Beal and Bryden 1999). Seasonal variability in the core flow's velocities has been observed by Krug and Tournadre (2012), with local minima observed in austral winter and maxima in austral summer. In-situ ocean currents measurements later confirmed the seasonal increase of the Agulhas Current flow in austral summer (Beal et al., 2015). These observations are in contrast with model simulation studies which show maximum in austral winter (e.g. Lutjeharms, 2006). On an annual timescale, the width of the Agulhas Current does not exhibit any temporal variations related to the core (Krug and Tournadre 2012). One study has suggested that over longer time scales of variability the Agulhas Current is widening (Beal and Elipot, 2016). The broadening is thought to be induced by intensifying winds that increase the EKE. This is contrary to the common hypothesis of the WBCs increasing in strength in response to the change in wind circulation regime thought to increase the mean flow of WBCs (Stommel 1948).

In the northern Agulhas Current, the shallow shelf widens from north of Cape St Lucia to the Durban offshore region with a width of about 50 km, forming the shelf region named the KwaZulu-Natal (KZN) Bight. Complex exchange between the colder shelf waters and the warm Agulhas Current waters is forced along this wider shelf (Lutjeharms 2006; Roberts et al. 2016). Near Cape St. Lucia, the current velocities can often exceed 2 $m.s^{-1}$ and decrease with the widening shelf downstream (Roberts et al., 2016). The offshore extent of the KZN bight limits the extent of the intense and warm current flow of the Agulhas Current on the shelf waters (Roberts et al., 2010) although instabilities along the shelf edge can develop and induce intrusion of plumes of warm waters onto the shelf (Gründlingh 1992). Roberts et al. (2010) showed the strong influence of the Agulhas Current jet flow on the shelf circulation processes and that the intrusion of the Agulhas Current onto the shelf could lead to shelf flow current speeds exceeding 1.5 $m.s^{-1}$ between Durban and East London. Roberts et al. (2010) moreover showed the presence of north-eastward currents along the coast between

the East London region and Durban. With a vertical extension of at least 600 m and maximum velocities reaching 1 $m.s^{-1}$, the north-eastward flow may have linkages with the Agulhas Undercurrent flow at about 800 m depth and a semi-permanent cyclonic feature off Durban (Roberts et al., 2010).

2.2 Agulhas Current's mesoscale variability

Mesoscale structures in the Agulhas Current range from 50 to 200 km including the popularly known large solitary meanders referred to as Natal Pulses (Elipot and Beal, 2015; Pivan et al., 2016). Natal Pulse events are associated with the Agulhas Current jet moving offshore from its mean position and the presence of an inshore cyclonic cold-core eddy (Lutjeharms, 2006; Leber and Beal, 2014). Natal Pulses are generated as a result of barotropic kinetic energy conversion from deep ocean eddies to the Agulhas Current jet (Tsugawa and Hasumi 2010). The Natal Pulses grow as they propagate downstream having a diameter of about 30 km at the generation site reaching up to 200 km near the Agulhas Bank, i.e. off Port Elizabeth (Rouault and Penven, 2011). Upstream, the phase speed of the Natal Pulse eddy is up to 20 $cm.s^{-1}$around the Natal Bight dropping to 5 $cm.s^{-1}$ past 34 °S (Rouault and Penven, 2011). Natal Pulses do not exhibit any distinct frequency in their temporal occurrence, with an average of one to two events per year reaching the latitude of Port Elizabeth (34◦S) (Rouault and Penven,2011).

Elipot and Beal (2015) estimated that a quarter of meanders do not make it through to the Retroflection region due to dissipation. In their study of Natal Pulses, Rouault and Penven (2011) noted a reduction in the number of Natal Pulses from the northern to the southern Agulhas Current regions. They attribute the discrepancy between the upstream and downstream number of eddies to along path dissipation. They showed that only a small proportion of eddies reaching the southern Agulhas Current are related to spawning of warm-core eddies at the Retroflection region in partial disagreement with previous studies (Schouten et al. 2002; Biastoch et al., 2008 b, a). In fact, most of the eddy shedding events

occur in isolation to the Natal Pulse events (Rouault and Penven, 2011; Elipot and Beal 2015). The passage of Natal Pulse does not appear to influence or change the Agulhas Current transport although it may modify the horizontal geometry of the jet by widening the Agulhas Current (Leber and Beal 2014).

Natal Pulse meanders exhibit an asymmetric horizontal velocity field with offshore velocities exceeding those in the inshore by twofold within both the surface and deep layers (Lutjeharms et al. 2003). The intensity of the cyclonic eddy circulation peaks when the maxima at all depths are vertically aligned (Pivan et al., 2016). The vertical extent of the Natal Pulse can reach the full depth of the Agulhas Current (Lutjeharms et al., 2001). Mesoscale eddies provide an efficient and generally dominant mechanism for cross-shelf exchange in the Agulhas Current associated with the propagation of anomalously warm water plumes and intrusion of waters onto the cold shelf region (Rouault and Penven 2011, Lutjeharms,2006; Krug et al., 2014). Pivan et al. (2016) also consider the presence of a north-eastward flow of warm water as complementary processes that enhance the cross-shelf exchange and mixing effect induced by Natal Pulse eddies. They further show that along this region, the 1000 m isobath has an abrupt change that leads to a loss in the large eddy's vertical coherence since the cyclonic eddy core roughly flows along this isobath. Pivan et al. (2016) describe the 1998 Natal Pulse as a combination of many smaller dynamical processes interacting with the larger Natal Pulse eddy creating a complex system on dynamical interaction.

Another smaller mesoscale eddy also observed in the northern Agulhas Current is the Durban Eddy. The Durban Eddy is a cold-core mesoscale eddy which occurs off Durban and exhibits north-eastward flows inshore of the KZN bight (Guastella and Roberts, 2016). The Durban Eddy exhibits a north-eastward counter-current on the inshore side often exceeding 1 $m.s^{-1}$ (Roberts et al., 2010; Guastella and Roberts, 2016). The Durban Eddy is driven by intense flows of the Agulhas Current along the shelf edge and can exist for 9 days on average (Guastella and Roberts, 2016). Guastella and Roberts (2016) gives the description of different

phases of the Durban Eddy of which the spin-up phase is the initial stage followed by maturation whereby the eddy intensifies and eventually breaks away and progress downstream where it fades as a lateral wave. Pearce (1977) suggested that the presence offshore Durban and intensification of the Durban Eddy is linked to the local topography via the generation of cyclonic vorticity during the intrusion of the Agulhas Current waters on the shelf. Satellite imagery and *in-situ* observations confirmed the cyclonic, semi-permanent eddy and its associated current reversal close to the coast (Roberts et al., 2010). Cyclonic circulation in the KZN bight can also occur independently of the presence or absence of the semi-permanent cyclonic Durban Eddy (Roberts et al., 2016).

2.3 Submesoscale processes in the Agulhas Current

Submesoscale structures are generated from larger mesoscale eddies, topographic forcing and strong meandering currents (McWilliams 2016). They are important for the dissipation of eddy kinetic energy and diapycnal mixing (Ferrari and Wunsch, 2009). One of the main mechanisms for the dissipation of energy in a WBC system occurs through interactions of the mean jet flow with the topography (Gula et al., 2016). In their study of the poleward flowing Gulf Stream, Gula et al. (2016) show that anticyclonic vorticity generated at the bottom boundary layer leads to the formation of submesoscale wakes, turbulence and increased diapycnal mixing. High submesoscale activity is a characteristic attribute of WBCs (Rudnick et al., 2015; Gula et al., 2015; Krug et al., 2017). The importance of submesoscale processes is highlighted greatly by model simulations (Klein and Shinoda, 2008; Gula et al., 2016).

Mantovanelli et al., (2017) provided evidence that short-lived local wind activity influences the generation and decay of cyclonic eddies by enhancing the horizontal shear instability. Lagrangian techniques revealed that the small eddies can trap and concentrate particles in their motion (Mantovanelli et al., 2017). Inshore cyclonic eddies can thus act as microclimate with entrained nutrients and fish larvae, and consequently enhanced biological productivity (Roughan et al., 2017). Shear edge cyclonic eddies generated in the absence of large solitary

meanders have been observed near the Agulhas Current inshore edge, over the steep slope of the continental shelf (Lutjeharms et al., 2003; Krug et al., 2017). Smaller submesoscale cyclonic eddies have also been observed offshore Port Elizabeth (Krug et al., 2017). One of the submesoscale cyclonic eddy observed by Krug et al. (2017) had a southward propagation speed of 37 $km.day^{-1}$. The impact of the submesoscale eddies is largely unknown due to a lack of observations. Krug et al. (2017) have shown evidence of isopycnal uplift associated with the passage of small meanders indicative of upwelling activity. Like their larger counterparts, these submesoscale eddies at the Agulhas Current front are often associated with warm plumes (Lutjeharms, 2006; Krug et al., 2017). The plumes generally have a strong SST signature in the inshore western edge of the cyclonic eddy (Krug et al., 2017).

2.4 Observation of the variability in the Agulhas Current

In the field of ocean observations, various tools and datasets such as SST imagery (Rouault and Penven 2011; Jury, 2015), altimetry (van Leeuwen et al., 2000), *in-situ* data (Rouault and Penven 2011; Elipot and Beal 2015; Krug et al., 2014 and 2017) and model experiments (Lutjeharms, 2006; Tsugawa and Hasumi, 2010) are combined for optimal analysis and quantitative understanding of the ocean variability. Various factors can affect the quality of the satellite observations including atmospheric aerosol, cloud coverage, land contamination, calibration and other technical challenges related to the sensor efficiencies (Martin et al., 2012). For large and mesoscale processes, satellite altimetry has relatively satisfactory performance in mapping the geographical variability of ocean surface circulation based on sea surface elevation (Beal et al., 2015). However, altimetry data, like other satellite products, is limited near the coastal region (50 – 100 km) and when imaging variability at short timescales (less than 10 days) (Beal et al., 2015). Geostrophic current velocities derived from altimetry observations may also suffer from spatial and temporal bias errors due to uncertainties in the spatial and temporal correlation analysis applied to reconstruct the 2D surface topography (Rio et al., 2005). The relatively small size and rapid evolutionary time of submesoscales present a barrier in their observation as many remote-sensing tools cannot

resolve very finite scales and *in-situ* observations are too sparse for detection of these structures (McWilliams, 2016).

The intrinsic nature of the dynamic circulation in intense boundary current systems poses a challenge for observations (Schaeffer and Roughan 2015). The scarcity of in-situ observations in the Agulhas Current has been mitigated to some extent through the use of complementary satellite observations. Combined *in-situ* and satellite observations studies in the Agulhas Current have helped improve our understanding of the Agulhas Current system. Krug et al. (2014) complemented Acoustic Doppler Current Profiler (ADCP) data with satellite altimetry to study and better represent the structure of the mesoscale meanders known as Natal Pulses. The use of spatially and temporally abundant data allowed for an improved spatial description of the variability induced by the Natal Pulse. The satellite observations are only reliable if they can represent ocean conditions accurately, this is verified during a process of validation through which satellite and in-situ data are compared.

CHAPTER 3 – DATA AND METHODS

In this chapter, we present the study domain and provide a description of the data, the processing, and the methods of analysis.

3.1. Study Area

Our domain of interest is presented in figure 3.1.1, including the coverage of the glider trajectories during two scientific experiments in 2015 and 2017.

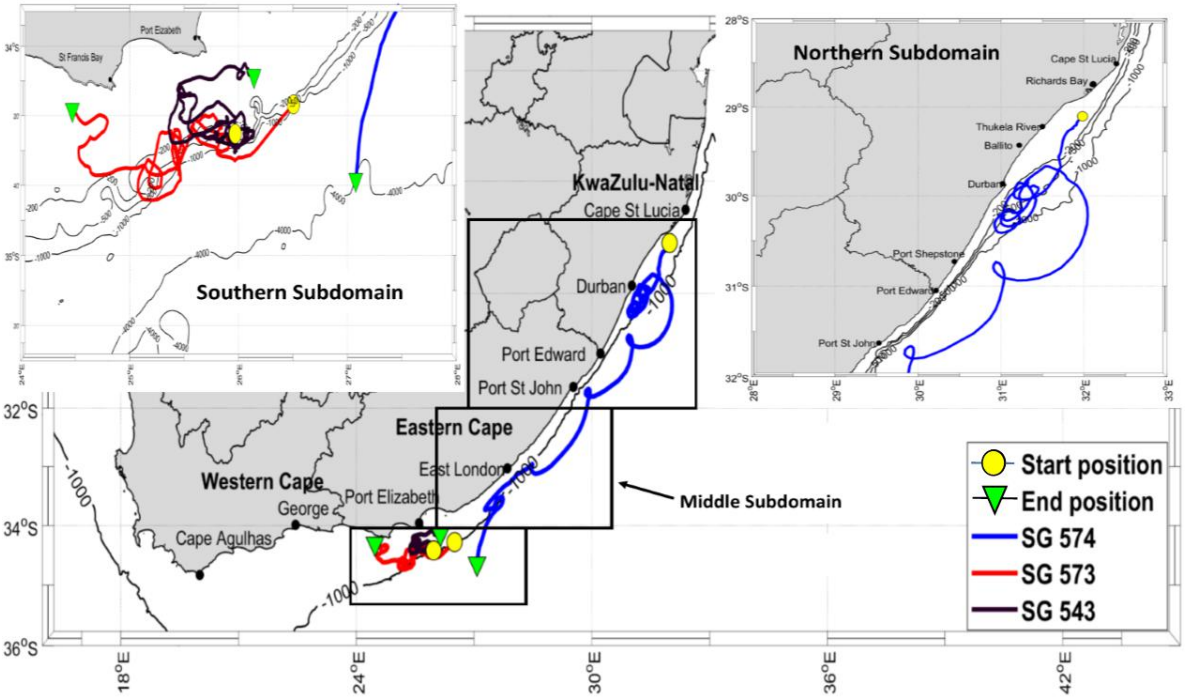

Figure 3.1.1: The bathymetry of the eastern and southern coasts of South Africa. The blue, red and purple lines indicate the glider paths for SG 574, SG 573 and SG 543 respectively with the green triangle (yellow circle) indicating the end (start) position of the glider. The northern (north of 32°S), middle (between 32°S and 34°S) and southern (south of 34°S) subdomains are demarcated by 3 boxes respectively.

The study domain has been divided into 3 subdomains with distinct oceanic processes and forcing. The northern subdomain (north of 32°S) encompasses the generation site for the Natal Pulse, the semi-permanent Durban Eddy, recirculation over the KZN bight and occasional perturbation by deep-sea eddies. The middle subdomain (between 32°S and 34°S) has a relatively narrow shelf for the most northern parts. The southern subdomain (south of 34° S) covers the region of a widening shelf downstream associated with an increase in

meandering and development of instabilities in the Agulhas Current (De Ruijter et al., 1999; Lutjeharms, 2006, Krug et al., 2014).

3.2. Glider data and processing

The in-situ data for our study were collected using gliders during the Shelf Agulhas Glider Experiment (SAGE: April-May 2015) and the Gliders in the Agulhas (GINA: June-August 2017) experiment (Krug et al., 2018). Gliders are underwater vehicles that control their buoyancy to sample the water column in vertical and horizontal dimensions (Rudnick et al., 2015). The Gliders used in our study sampled between the surface and 1000 m depth. Data from 3 gliders, seaglider (SG) 574 from GINA and 2 gliders from SAGE namely SG 573 and SG 543, are used in this study. Measurements were taken at varying frequencies according to the sensors and depth levels i.e. high sampling frequency at shallow depths and lower sampling frequency for greater depths. In accordance with the sampling frequencies, the vertical profile data from the CTD sensor were gridded to 0.5 m for the first upper 100 m, then to 1 m down to 200 m depth, and finally to 2m for depths greater than 200 m. The data were transmitted to a satellite receiver after each dive, in real-time via wireless telemetry. During the data transmission, instruction commands like location, change of sampling trajectory, sensor configuration etc. are provided to the glider from a remote operational base. The gliders were equipped with a Conductivity, Temperature and Depth sensor (CTD), and sensors for other variables including chlorophyll and dissolved oxygen. All the sensors attached to the gliders were calibrated prior to deployments. The initial glider data processing was done by the Applied Physics Lab (APL) at the University of Washington and it includes, mainly, high resolution signal processing.

Surface and depth-averaged velocity estimates

The depth-averaged currents derived from ocean glider observations are estimated from the comparisons of the distance covered by the glider and the positional data in the subsurface using the dead reckoning technique (Rudnick et al., 2015). In contrast, surface currents are

estimated from the glider's drift at the surface before the start of a dive cycle (e.g. Krug et al., 2017).

GPS position coordinates are captured at the end and start of each dive cycle. Depending on the ocean conditions at the sea surface, the position of the glider can change significantly while the satellite connection is being established. The major source of errors in the glider-based current speed and direction measurements arises from the capturing of the location within a reasonable spatial accuracy in both horizontal and vertical extents (Rusello et al., 2012). Other sources of error such as bias errors from physical rotation and inaccurate speed of sound exhibit a cumulative growth with time and can lead to a similar magnitude of error in the logged final position. Typically, the uncertainties of glider-based current velocity estimates for the surface and depth-averaged velocities are in the orders of 0.05 m/s and 0.01 m/s, respectively, with a 10 m GPS accuracy (Eriksen et al., 2001; Rudnick et al., 2015; Krug et al., 2017). In this study, only the surface current measurements from the gliders are used to compare with the satellite GlobCurrent estimates and throughout the study i.e. glider current measurements refer to the surface currents measurements. The processing and quality control of the glider's surface current dataset involved computing the differences in current speeds exceeding 1 $m.s^{-1}$ between the 3-hour running mean and the raw surface current velocities to identify and remove outliers from the glider-based velocity estimates. The duration of each dive varied depending on the maximum encountered depth, implying that deeper dives had a longer duration than shallow dives. On average dives lasted for about 1 hour.

3.3. Satellite data and processing

3.3.1. GlobCurrent current data

Ocean current data from the GlobCurrent portal (http://www.globcurrent.org) are used in this study. GlobCurrent products include geostrophic currents and Ekman currents (at either 0m or 15 m) and their combination at a spatial and temporal resolution of 25 km and 3 hourly to daily. GlobCurrent data is available from 1993 to present. The Ekman currents are derived

using data from surface drifters, Argo floats and ECMWF surface winds products to produce gridded data at a 3-hourly temporal resolution. The methods used to derive both the Ekman and geostrophic currents are described in Rio et al. (2014). A combined ocean current product made of Ekman and geostrophic (product termed Total) is also provided at a 3-hourly temporal resolution. The Ekman and the Total currents are provided at two depth levels: 0m and 15m. Only the combined Ekman current measurements at the 15m depth and the geostrophic current measurements are used mainly in this study. Beyond the time series comparisons, only the Total currents at 15m depth are used. An important note about the GlobCurrent data is that the 3-hourly temporal resolution is the output resolution from a temporally and spatially interpolated dataset. Note that the effective resolution of the surface geostrophic current products derived from altimetry data is closer to 10 days and the resolved spatial scales are in the 50-100 km range (Ubelmann et al., 2015).

3.3.2. ODYSSEA Sea Surface Temperature data

The satellite SST product used in our study is obtained from ftp://eftp.ifremer.fr/cersat-rt/project/medspiration/data/l4/. The SST fields (ODYSSEA) are a Level 4 product produced by merging of observations from infrared and microwave satellites including the Advanced Along Track Scanning Radiometer (AATSR), the Moderate Resolution Imaging Spectroradiometer (MODIS) the Advanced Very High-Resolution Radiometer (AVHRR) and the Advanced Microwave Scanning Radiometer (AMSR-2). These source SST fields have resolutions of about 1 km (infrared) and 25 km (passive microwave). The product utilizes optimal interpolation techniques to produce cloud- and gap-free SST fields at a daily temporal resolution. The L4 SST fields represent the foundation SST's which are independent of the diurnal fluctuations due to radiation or wind effects. The gridded SST maps, with a resolution of 2 km, are used to identify and track mesoscale features.

3.3.3. Bathymetry data

The bathymetry data used in this study were obtained from the General Bathymetric Chart of the Oceans (GEBCO). The GEBCO_2014 Grid is developed from observations of ship soundings and interpolated with a continuous terrain model for lands and oceans at 30 arc-

sec resolution. The interpolation methods also include gravity date derived from satellites. More information and access to the data can be found at http://www.gebco.net/data_and_products/gridded_bathymetry_data/

3.4 Methods for analysis

For the time series analysis, daily averages of the meridional and zonal components of the current speeds derived from the gliders were calculated and compared to the daily GlobCurrent products of combined Ekman and geostrophic currents (Total) at 15m. Glider SSTs are extracted from individual dives and averaged within the upper 3 meters from the surface and at daily intervals before comparisons with daily SSTs from ODYSSEA. The mean values and the standard deviation used as a measure of the measurements variability are reported in this format: mean (standard deviation represented by s).

The method of co-locating GlobCurrent data with daily averaged positions of the gliders is done by finding the closest grid point to the daily averaged glider positions. Distances between GlobCurrent and glider point observations and the 1000 m isobath position, extracted from the GEBCO dataset, are calculated to represent the relative cross-shelf position of the glider and GlobCurrent observations. The method used for cross-shelf binning of glider data in reference to the 1000 m involves creating 1km intervals on either side of the 1000 m isobath to create cross-shelf bins with 1km width. The glider data and corresponding satellite data source data are then allocated to the relevant bins in line with their longitude and latitude information. An average is calculated for every bin across the shelf region for the available data and according to the defined latitudinal limits of the subdomains. A more detailed description of the cross-shelf binning method is provided in Krug et al., (2017). The 1000 m isobath is chosen because the inshore edge of the Agulhas Current is found along this isobath (e.g. Krug et al., 2017). All the statistical tests including correlation test and student t-test are conducted at the 5% significance level i.e. $\alpha = 0.05$.

CHAPTER 4: RESULTS

In this Chapter, the key findings and results are presented. In section 4.1, the satellite observations are compared to the *in-situ* observations to assess GlobCurrent's ability to capture variability in the Agulhas Current speeds as well as the accuracy of the GlobCurrent product in the Agulhas Current region. In Section 4.2, we investigate the ability of the GlobCurrent product to capture the mean cross-shelf flow over different Agulhas Current sub-regions. In Section 4.3, case studies of a Natal Pulse and a Durban Eddy are used to evaluate how GlobCurrent represents mesoscale processes. Finally, in section 4.4 we investigate if synergies with merged SST products, such as ODYSSEA SST can improve our ability to monitor the Agulhas Current from space.

4.1. Accuracy and variability depicted in the GlobCurrent product in comparisons to glider observations:

The time series of the glider-based current speed for SG 543 and the corresponding GlobCurrent speeds (figure 4.1.1. a) show glider current speeds to be lower, mostly, than the GlobCurrent current speed estimates. Notably, a steep increase to the maximum value recorded by the glider between May 1st and May 2nd is not present in the GlobCurrent series. Maximum and minimum values of 1.6 $m.s^{-1}$ and 0.23 $m.s^{-1}$ on May 2nd and April 24th are recorded by the glider, respectively. The corresponding, collocated GlobCurrent satellite-derived current speeds depict a minimum value of 0.36 $m.s^{-1}$ for both geostrophic and Total 15m current speed components. The geostrophic current speed records a maximum of 1.15 $m.s^{-1}$ on May 2nd and 1.07 $m.s^{-1}$ is reported for the Total 15m component on May 19th. The Ekman component of the flow showed very little variation throughout the duration of the glider mission with maximum values barely exceeding 0.1 $m.s^{-1}$. For all glider current data, we refer to the Total 15m current as GlobCurrent hereafter. The difference between the glider speeds and GlobCurrent was statistically significant at the 95% confidence interval and using a paired student t-test (geostrophic with p-value = $5.31\ x\ 10^{-9}$ and t-stat =7.55; GlobCurrent with p-value = $4.59\ x\ 10^{-8}$ and t-stat = 6.76).

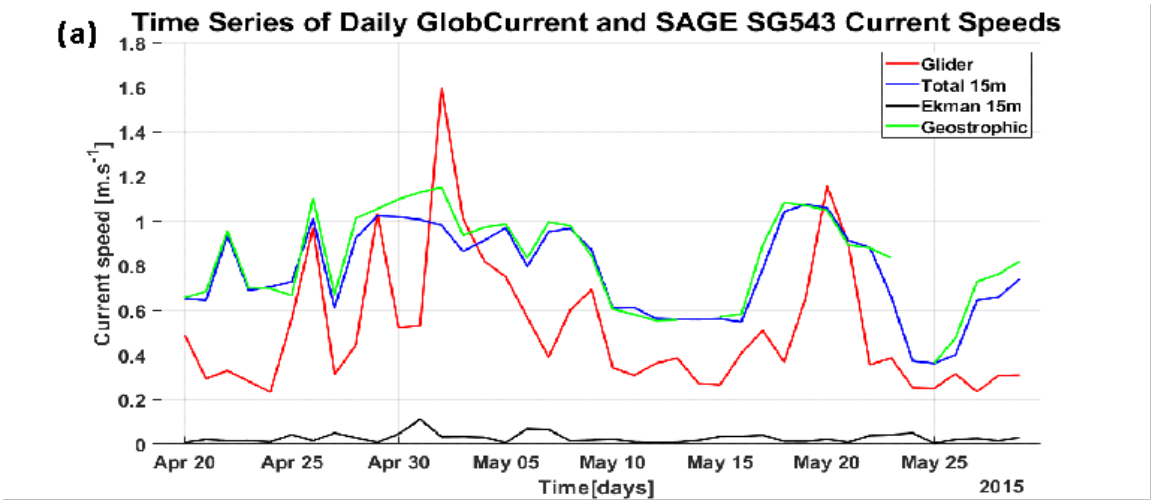

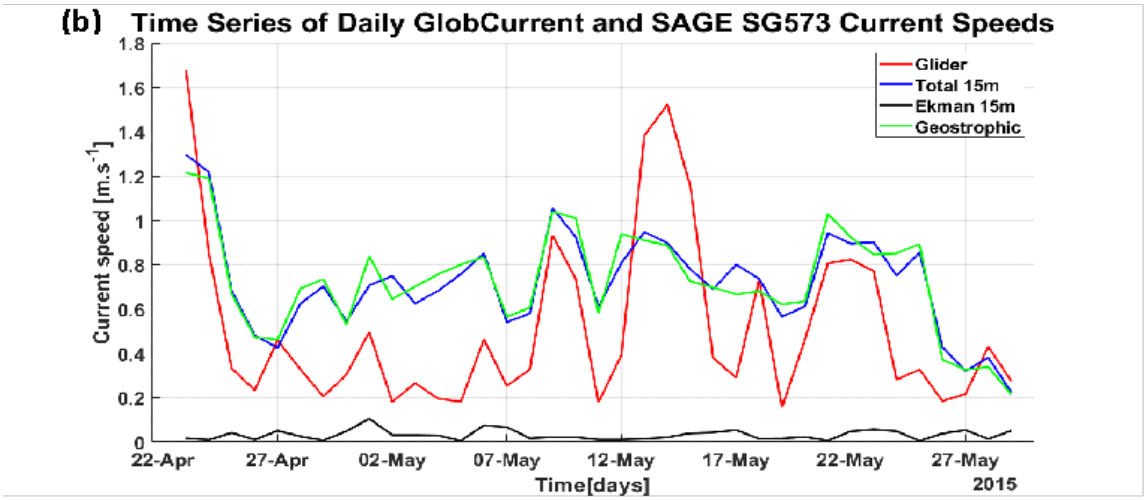

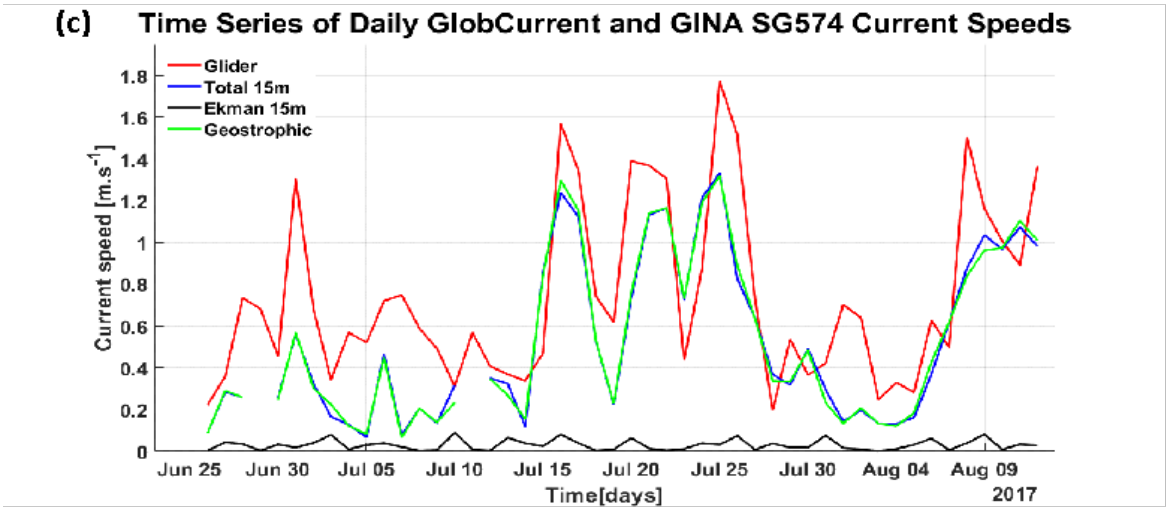

Figure 4.1.1 Time series of daily current speeds extracted from the glider and GlobCurrent datasets. The following GlobCurrent current speed products are plotted: Total at 15m, Ekman 15m, and Geostrophic. Comparisons are made with glider data from (a) SG 543 - SAGE 2015, (b) SG 573 - SAGE 2015 and (b) SG 574 - GINA 2017 gliders. Each dataset is associated with a unique colour as shown in the plots legends.

The GlobCurrent mean current speed was 0.77 $m.s^{-1}$ (s =0.20 $m.s^{-1}$) in comparison to an average of 0.52 $m.s^{-1}$ (s =0.30 $m.s^{-1}$) for the glider observations. With a mean bias of 0.25

$m.s^{-1}$ corresponding to about 49% difference, the percentage ratio of GlobCurrent RMSE to glider RMSE has a value of 67%. This indicates that there is significantly more variability in current speed daily averages from the glider data than from the GlobCurrent estimates. Despite these differences, GlobCurrent's patterns of current speed increase and decrease are generally in agreement with the glider. The GlobCurrent and glider current speeds are correlated with a correlation coefficient of 0.63 significant at the 95% confidence level (p-value =1.31^{-5}) from a 2-tailed correlation test.

A similar pattern of lower maximum current speed values for GlobCurrent estimates but greater averaged current speeds is also found in our comparisons with the SG573 record (figure 4.1.1. b). The records start with a glider maximum current speed of 1.68 $m.s^{-1}$ on April 23rd with GlobCurrent estimates recording a maximum of 1.3 $m.s^{-1}$ on the same day as the glider. The glider shows a steep decrease in the current speed of about $0.87\ m.s^{-1}$ in the first 5 days of sampling. The GlobCurrent current speed records reach a minimum on May 29th with the current speed value of 0.21 $m.s^{-1}$. A minimum current speed of 0.15 $m.s^{-1}$ is observed on May 19th. The mean values for the glider and GlobCurrent current speeds are 0.52 $m.s^{-1}$ (s =0.40 $m.s^{-1}$) and 0.72 $m.s^{-1}$ (s =0.23 $m.s^{-1}$) respectively. The difference in mean values between the SG 573 and GlobCurrent was statistically significant at the 95% confidence level (t-sat = 4.19 ;p-value = $1.68\ x\ 10^{-4}$). On May 14th, SG 573 recorded the second-highest maximum current speed with a value of 1.52 $m.s^{-1}$ while the GlobCurrent current speed recorded a value of about 0.89 $m.s^{-1}$on the same day. A statistically significant correlation with a correlation coefficient of 0.69 was found between the SG 573 and GlobCurrent current speed records (p-value = $2.5\ x\ 10^{-6}$). GlobCurrent exceeded the glider-based current speed records by 39% with a mean bias of 0.2 $m.s^{-1}$. The percentage ratio of the RMSE of the glider to GlobCurrent current speeds for SG 573 had a value of about 58%, the lowest of all three gliders.

SG 574 glider was deployed further north along the east coast in different waters to SG 543 and SG 573 gliders (see figure 3.1.1). The SG 574 and GlobCurrent records of current speed

presented on a time series (figure 4.1.1. c) were generally coherent. The first local peak from the start of the glider mission was reached on July 1st with a current speed of 1.3 $m.s^{-1}$ and 3 consecutive peaks follow starting from July 14th to July 28th with a maximum of 1.77 $m.s^{-1}$ on July 25th; this was the maximum daily speed for the whole glider record. Throughout the duration of the glider mission, the glider appeared to register higher values than the GlobCurrent record. Notable discrepancies were seen from July 31st to August 3rd, when the local peak in glider speed on August 1st was not represented in the GlobCurrent record. Another glider peak on August 8th was also not captured in the GlobCurrent record, including the increasing speed from August 11th to 12th. With a mean speed of 0.74 $m.s^{-1}$ (s =0.42 $m.s^{-1}$), the glider current speeds were significantly greater, on average, than the GlobCurrent observations which had a mean value of 0.52 $m.s^{-1}$(s =0.39 $m.s^{-1}$; t-stat= -5.48; p-value= $1.83\ x\ 10^{-6}$). Both time-series were correlated with a correlation coefficient of 0.79, significant at the 95% confidence level (p-value= $1.01\ x\ 10^{-10}$). The mean bias between SG 574 and GlobCurrent was 0.21 $m.s^{-1}$ which corresponds to -29 % difference and a % RMSE of 90%, the highest of all three gliders. This high %RMSE indicates that variations around the mean values were similar in both the GlobCurrent and glider(SG 574) time series. When using all the glider data by combining records from SG543, SG573 and SG574, a correlation coefficient of 0.55 (p-value= $4.16\ x\ 10^{-11}$) was found, with a mean current speed of 0.66 $m.s^{-1}$, a mean bias of 0.06 $m.s^{-1}$and a %RMSE of 79%.

The scatter plot of current speeds from both *in-situ* and satellite observations in figure 4.1.2 represents all paired observations from the glider and corresponding GlobCurrent current speed observations. Values below (above) the y= x line indicate where GlobCurrent current speeds are greater (less) than glider current speeds. For most observations collected over water depths shallower than 250 m (dark red circles), GlobCurrent appears to be overestimating the current speed values.

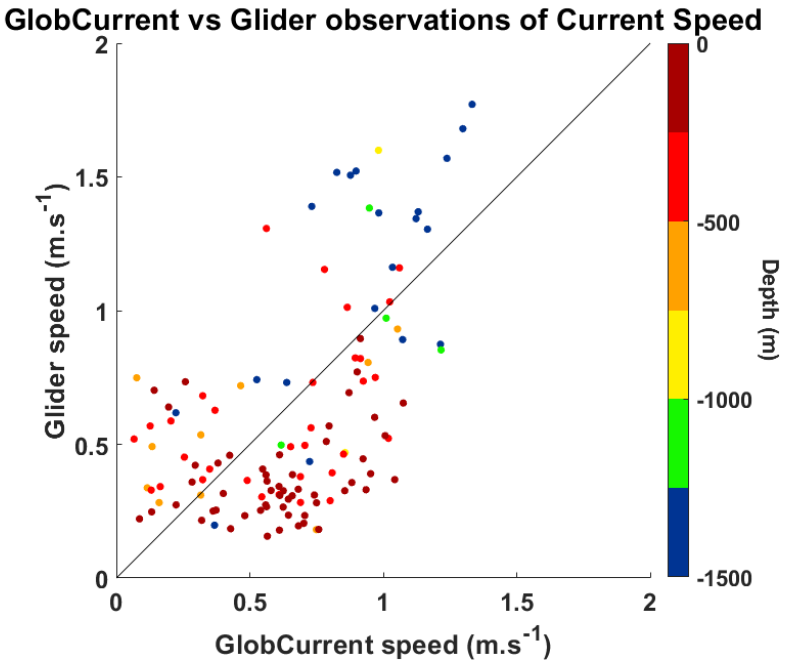

Figure 4.1.2 Scatter plot of co-located GlobCurrent and Glider current speeds with the colours representing the depth of the water column at the location where the glider was sampling. The water depth was derived using the glider coordinates by extracting the water depth at each location from the GEBCO bathymetry. The diagonal line represents the line y = x, where a perfect agreement is found.

Only about 4 data points are in perfect agreements and lie exactly on the y=x line. In water depths ranging from 500m to 750m (orange circles) and in deeper waters (mostly > 1000 m) (blue circles), GlobCurrent underestimates the values of current speed. Importantly, GlobCurrent current speed observations never exceed 1.35 $m.s^{-1}$whereas glider observations reach up to 1.77 $m.s^{-1}$. These high current speed values are observed in deeper waters (> 1000 m) indicating proximity to the inshore edge of the Agulhas Current front. In general, GlobCurrent is overestimating surface current speeds in shallower waters (<500m) although there are notable observations with lower current speed from GlobCurrent than glider records.

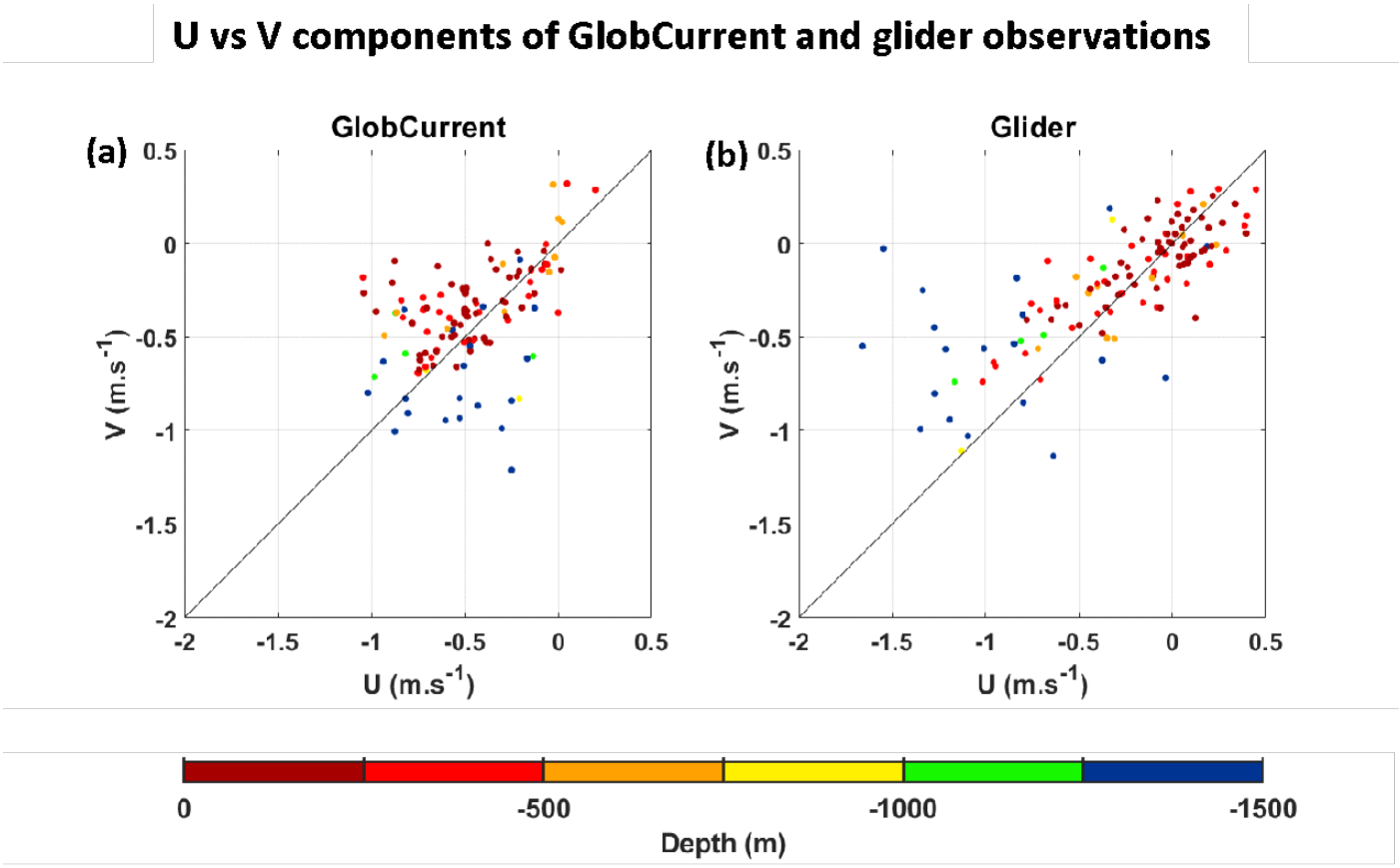

Figure 4.1.3: Scatter plot of the zonal versus meridional components of current flows from (a) GlobCurrent and (b) Glider surface current observations; the colours represent the associated water depth extracted from the GEBCO bathymetry.

Extending the GlobCurrent and glider comparisons, we present scatter plots of the zonal (U) and meridional (V) current components for each of the data sources (figure 4.1.3). GlobCurrent observations (figure 4.1.3.a) are generally more clustered with most current speeds between 0 $m.s^{-1}$ and -1 $m.s^{-1}$ for both the meridional and zonal components. Observations in deeper waters, i.e. > 750 m, exhibit a flow with a stronger meridional current component than in shallow water where the zonal flow dominates the general flow. Points with positive U and V values in depths between 250 m and 750 m shown in Figure 4.1.3(a) indicate a north-east or northward flow. The GlobCurrent scatter plot of U and V velocities does not clearly reveal the major flow axis. Glider observations (figure 4.1.3 b), on the contrary, exhibit a more diagonal spread along the y=x line. For the glider data, both U and V points are clustered around 0.5 $m.s^{-1}$ and -0.5 $m.s^{-1}$. Furthermore in the combined glider record, flows in shallow water (<250m) are predominantly towards the north-east while deeper flows are toward the south-west with a fairly strong westward component. Generally,

shallow water glider observations show current components with values barely exceeding 0.5 $m.s^{-1}$. In deeper waters, the meridional component of the flow in the GlobCurrent product was stronger than that observed from the gliders. The discrepancies between the glider-based observations and the GlobCurrent observations were shown to have directional errors in addition to the magnitude of the current speed.

4.2 Regional and cross-shelf circulation in the GlobCurrent product

The time averaged cross-shelf data from the gliders and the corresponding GlobCurrent measurements collocated in time and space is presented in figure 4.2.1. Figure 4.2.1 shows all three subdomains over which the time-averaged cross-shelf vectors are computed.

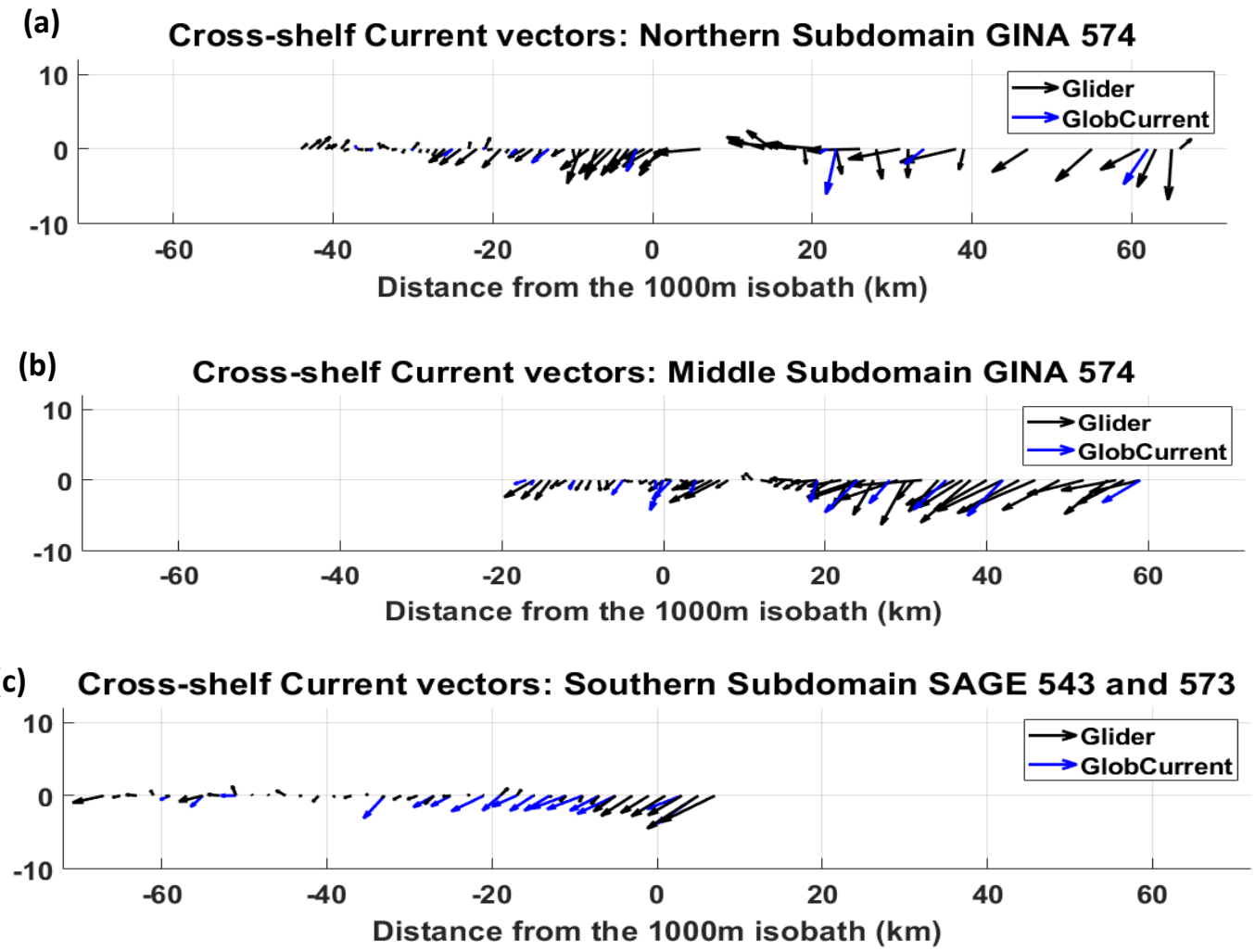

Figure 4.2.1: Cross-shelf current vectors from glider observations and GlobCurrent in the (a) Northern, (b) Middle and (c) Southern Subdomains. The horizontal axis indicates the distance (km) from the 1000 m isobath with increasing negative values towards the coastline.

Due to the relatively limited number of glider observations and the fairly coarse spatial resolution of the GlobCurrent dataset, only a few GlobCurrent cross-shelf vectors are present in the final time-averaged cross-sections. The time-averaged vectors in figure 4.2.1(a) exhibit an inshore-offshore gradient of current speed. Low current speed values with an inshore oriented flow are observed about 20 km inshore of the 1000 m isobath. Closer to the coast, a contrasting flow with a north-eastward direction is notable. Minimum speed values can be seen about 30 km inshore from the 1000 m isobath (figure 4.2.1 a). Strong south to south-westward flows are shown on the seaward side of the 1000 m isobath. The GlobCurrent minimum and maximum speed values were 0.09 $m.s^{-1}$ and 1.24 $m.s^{-1}$, respectively. This is different from the 0.22 $m.s^{-1}$ and 1.7 $m.s^{-1}$ respective minimum and maximum values from the glider observations. For both GlobCurrent and glider observations, the minimum and maximum current speed values were observed near 40 km landward and 20 km seaward of the 1000 m isobath. Strong shoreward flow is shown 10 km to 20 km seaward of the 1000 m isobath (figure 4.2.1 a).

A strong flow on the seaward side of the 1000 m isobath is also exhibited in figure 4.2.1 (b). There is a clear inshore-offshore current speed gradient with low current speeds near the shore and higher current speeds further offshore. The flow direction for the middle subdomain (figure 4.2.1 b) is oriented along a northeast-southwest axis in the direction of the isobaths. The GlobCurrent (glider) minimum current speed is found about 16 km (5 km) on the landward side of the 1000 m isobath with a value of 0.15 $m.s^{-1}$ (0.16 $m.s^{-1}$) as shown in figure 4.2.1(b). The maximum current speeds, for both GlobCurrent and glider datasets are associated with a south-westward flow located about 40 km from the 1000 m isobath, on the seaward side. About 5 km in the seaward direction from the 1000 m isobath, glider current speed observations peak, locally, at 1.23 $m.s^{-1}$, Note that GlobCurrent data is not available at this location (Figure 4.2.1 b). Past 20 km, seaward from the 1000 m isobath, both the glider and GlobCurrent current speed values increase sharply although the GlobCurrent values remain below the glider measurements. The lower subdomain only contains the 2015 datasets from the SAGE glider missions. Figure 4.2.1 (c) shows the current

vectors in the Agulhas bank region. The maximum current speeds are recorded around 5 km from the 1000 m isobath on the seaward side of the 1000 m isobath with values 1.3 $m.s^{-1}$and 1.5 $m.s^{-1}$ for GlobCurrent and glider datasets respectively (figure 4.2.1 c). From the location of the maximum current speed moving landward, up to 10 km from the 1000 m isobath, there is an agreement in the direction of the flow between GlobCurrent and glider records although the glider magnitude registers higher values than GlobCurrent. Few glider observations were collected between the coast and 40 km inshore of the 1000 m isobath and caution should be exercised when interpreting the cross-shelf time average. In General, GlobCurrent underestimated the current speed values near the 1000 m isobath (7 km seaward and 5 km landward) and overestimated the current speed between within 7km to 33 km from the 1000 m isobath on the landward side (figure 4.2.1 c). The data points collected in this coastal region were collected at a time when the gliders were caught around submesoscale eddies and this cross-shelf section is therefore not representative of a long term time-average. Landward, beyond the 33 km point inshore of the 1000 m isobath there are very few GlobCurrent data points to compare with glider data (figure 4.2.1 c).

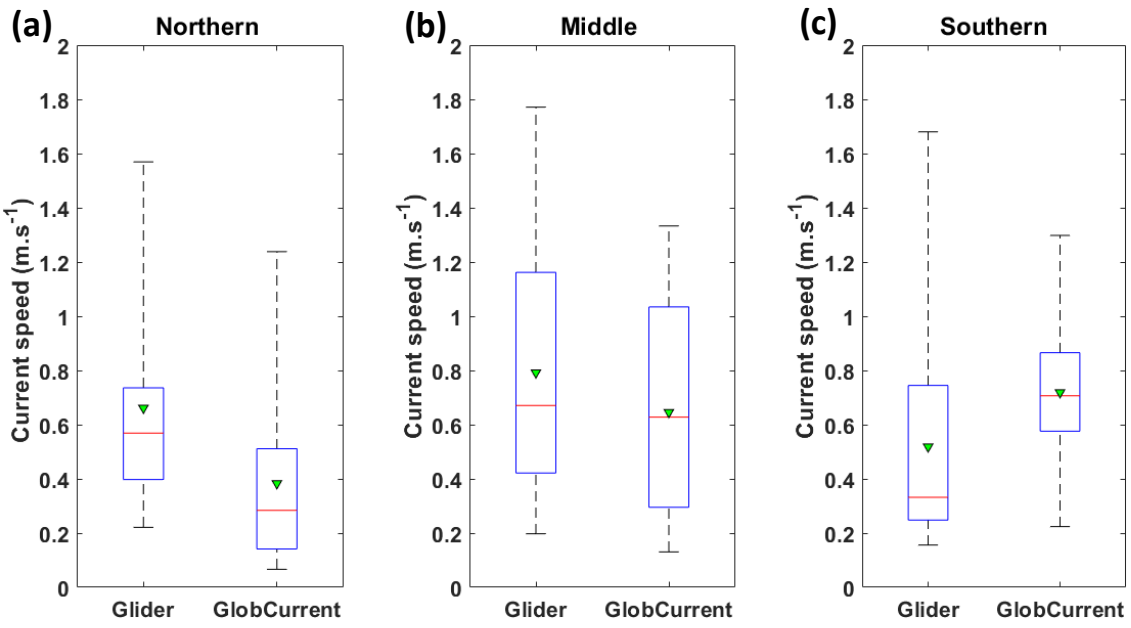

Figure 4.2.2: Boxplot of surface current speed from glider data and GlobCurrent estimates in the (a) Northern < 32°S, (b) Middle 34 > & > 32°S and (c) Southern > 34°S subdomains. The red line and green triangle mark the median and mean values respectively. The blue box represents the interquartile range; lower quartile (Q1) at the bottom and upper quartile (Q3) at the top. The dashed lines represent data points outside the interquartile range.

Figure 4.2.2 shows a boxplot of the current speed from glider data and GlobCurrent estimates in the 3 different subdomains; northern, middle and southern subdomains. The northern subdomain (figure 4.2.2 a) has all the glider data north of 32°S and corresponding GlobCurrent observations, the middle subdomain (figure 4.2.2 b) cover observations between 32°S and 34°S, and lastly the southern subdomain (figure 4.2.2 c) has all observations south of 34°S. The northern subdomain (figure 4.2.2 a) shows a positively skewed distribution of the current speed for both glider and GlobCurrent. About 75% of the glider observations lie below 0.74 $m.s^{-1}$ with a standard deviation of 0.42 $m.s^{-1}$. For GlobCurrent, the 75% mark is at 0.51 $m.s^{-1}$ with 0.38 $m.s^{-1}$ as the standard deviation. Maximum values are 1.24 $m.s^{-1}$and 1.57 $m.s^{-1}$; minimum values are 0.09 $m.s^{-1}$ and 0.22 for the GlobCurrent and glider data respectively. The glider mean value of 0.75 $m.s^{-1}$ (s =0.42 $m.s^{-1}$) is significantly greater than the GlobCurrent mean of 0.47 $m.s^{-1}$ (s =0.38 $m.s^{-1}$). This difference is significant at the 95% confidence level (t-stat= -5.41; p-value = $1.97\ x\ 10^{-5}$). The middle subdomain (figure 4.2.2 b) has a distinctly different distribution to the northern subdomain. The glider box plot exhibits a slightly positively skewed distribution with a longer whisker toward the right (up) contrary to the GlobCurrent boxplot that appears similar to a normal distribution. The mean value and the median value are almost equal for GlobCurrent and more different for the glider observations. The GlobCurrent and glider datasets in the middle subdomain have maximum current speeds of 1.33 $m.s^{-1}$ and 1.77 $m.s^{-1}$, and minimum speeds of 0.15 $m.s^{-1}$ and 0.2 $m.s^{-1}$, respectively.

There is a significant difference (t-stat= -2.41 ;p-value= 0.025) between the closely similar mean value of 0.65 $m.s^{-1}$ (GlobCurrent, s =0.41 $m.s^{-1}$) and 0.79 $m.s^{-1}$ (Glider, s =0.47 $m.s^{-1}$). The 75% quartile is marked at 1.16 $m.s^{-1}$ and 1.03 $m.s^{-1}$ for glider and GlobCurrent respectively. The GlobCurrent dataset in the southern subdomain (figure 4.2.2 c) shows a relatively normal distribution of current speed, while the glider current speed distribution is positively skewed. The GlobCurrent minimum and maximum values fall within the range of glider observations. With minimum speed of 0.27 $m.s^{-1}$ and 0.18 $m.s^{-1}$; maximum speeds of 1.26 $m.s^{-1}$ and 1.29 $m.s^{-1}$, the southern subdomain exhibits a distinctive pattern that is

almost opposite to that of the northern domain. The GlobCurrent observations have a mean value of 0.75 $m.s^{-1}$ (s =0.22 $m.s^{-1}$) which is significantly greater than the 0.52 $m.s^{-1}$ (s =0.35 $m.s^{-1}$) mean value from the glider dataset (t-stat= 7.58; p-value= $6.85\ x\ 10^{-11}$). The GlobCurrent observations have almost equal data points on either side of the mean and median. About 75% of the GlobCurrent data lies below 0.92 $m.s^{-1}$ in contrast to 0.7 $m.s^{-1}$ for the gliders. For all the subdomains, mean bias values of 0.28 $m.s^{-1}$, 0.12 $m.s^{-1}$ and 0.2 $m.s^{-1}$ corresponded to percentage difference values of -37%, -15% and 29% for the northern, middle and southern subdomains respectively. Furthermore, the RMSE ratio for glider to GlobCurrent values were 86%, 81% and 68% for northern, middle and southern subdomains respectively. The northern(southern) subdomain had the highest(lowest) RMSE ratio compared to the other subdomains. A summary of current speed statistics for both glider and GlobCurrent datasets is presented in Table 4.1.1.

Table 4.1.1 Summary statistics of all the time-series and subdomains current speed data from in-situ glider and satellite GlobCurrent. The 2nd – 5th columns show the minimum, maximum, mean and standard deviation computed from each co-located glider and GlobCurrent time-series. From the 6th to the 9th columns, the mean bias, percentage difference, percentage RMSE, correlation and the p-value for the correlation are calculated from GlobCurrent-glider pairs at corresponding times, locations and subdomains. Northern sub., Middle sub. and Southern Sub. represent the (a) Northern < 32°S, (b) Middle 34 > & > 32°S and (c) Southern > 34°S subdomains.

Data Source	Min ($m.s^{-1}$)	Max ($m.s^{-1}$)	Mean ($m.s^{-1}$)	Standard deviation ($m.s^{-1}$)	Mean bias ($m.s^{-1}$)	% Difference	% RMSE	Correlation (r)	p-value (corr)
SG 543	0,23	1,6	0,52	0,3					
GlobCurrent(543)	0,36	1,07	0,77	0,2	0,25	48,53	67,04	0,63	1,31E-05
SG 573	0,16	1,68	0,52	0,4					
GlobCurrent(573)	0,22	1,3	0,72	0,23	0,2	38,63	57,95	0,69	2,50E-06
SG 574	0,2	1,77	0,74	0,42					
GlobCurrent(574)	0,07	1,33	0,52	0,39	-0,21	-29,1	90,03	0,79	1,01E-10
Northern sub. (Glider)	0,22	1,57	0,66	0,36					
Northern sub. (GlobCurrent)	0,07	1,24	0,38	0,33	-0,28	-37,46	86,34	0,89	1,24E-04
Middle sub. (Glider)	0,2	1,77	0,79	0,47					
Middle sub. (GlobCurrent)	0,13	1,33	0,65	0,41	-0,12	-15,11	81,12	0,81	3,86E-04
Southern sub. (Glider)	0,16	1,68	0,52	0,35					
Southern sub. (GlobCurrent)	0,22	1,3	0,75	0,22	0,2	38,74	74,13	0,8	2,32E-06
All Gliders	0,16	1,77	0,6	0,39					
All GlobCurrent	0,07	1,33	0,66	0,31	0,06	9,97	78,84	0,55	4,16E-11

4.3 Ability to capture mesoscale variability: Meanders and eddies

Case studies of mesoscale features presented in this section are extracted from the 2017 GINA glider dataset. This specific dataset was used following the high correlation strength and a higher %RMSE between the glider and GlobCurrent datasets. Extending the analysis to the observations of large (>100 km) and smaller (50-100 km) mesoscale structures, SST maps are used to identify surface features. Time series of the glider's CTD profiles are used to illustrate the vertical structure of mesoscale features. The analysis is presented in two subsections, (4.3.1) small mesoscale features in shallow water (< 500m) and (4.3.2) larger mesoscale structures in deeper waters (predominantly > 1000 m).

4.3.1. Case study of the Durban Eddy

Figure 4.3.1 shows SST maps over the narrow shelf of the Natal Bight region. Figure 4.3.1 (a) shows the glider making the first clockwise turn on June 28th. The normalized current vectors exhibit a pattern indicating an inshore flow between 29°S and 30°S, in contrast to the predominantly south-westward flow over the rest of the region. Cool coastal waters with low SST values with a minimum of about 20.2 ℃ (figure 4.3.1 f) are in clear contrast with Agulhas Current waters reaching a local maximum exceeding 23.5 ℃ (figure 4.3.1 e). A patch of low SST around 30°S where the glider makes a rotating pattern shows a weak temperature contrast to the surrounding waters on June 30th. Between June 26th and July 10th, the glider is caught in a cyclonic eddy (the Durban Eddy). While the GlobCurrent and the glider derived surface currents are in relatively good agreement when the glider is on the seaward side of the cyclonic eddy and traveling towards the south-west, the GlobCurrent product is not able to capture the north-easterly flow experienced by the glider on the inshore cyclonic eddy side, near 30° S - 31° E. GlobCurrent vectors highlight the larger circulation structure but do not capture the small eddy sampled by the glider at 31° E. From July the 10th onwards, the glider continues in a north-eastward direction and is then entrained into a larger mesoscale eddy captured in both the GlobCurrent and SST datasets (figure 4.3.1 e and f). From June 25th to around July 13th, the glider spends most of the time in waters shallower than 500m (Figure

4.3.2 b). About 4 days from the start of the time series, the glider is confined to shallow waters of ≈50m with speed values not exceeding 0.6 $m.s^{-1}$ (Figure 4.3.2 a).

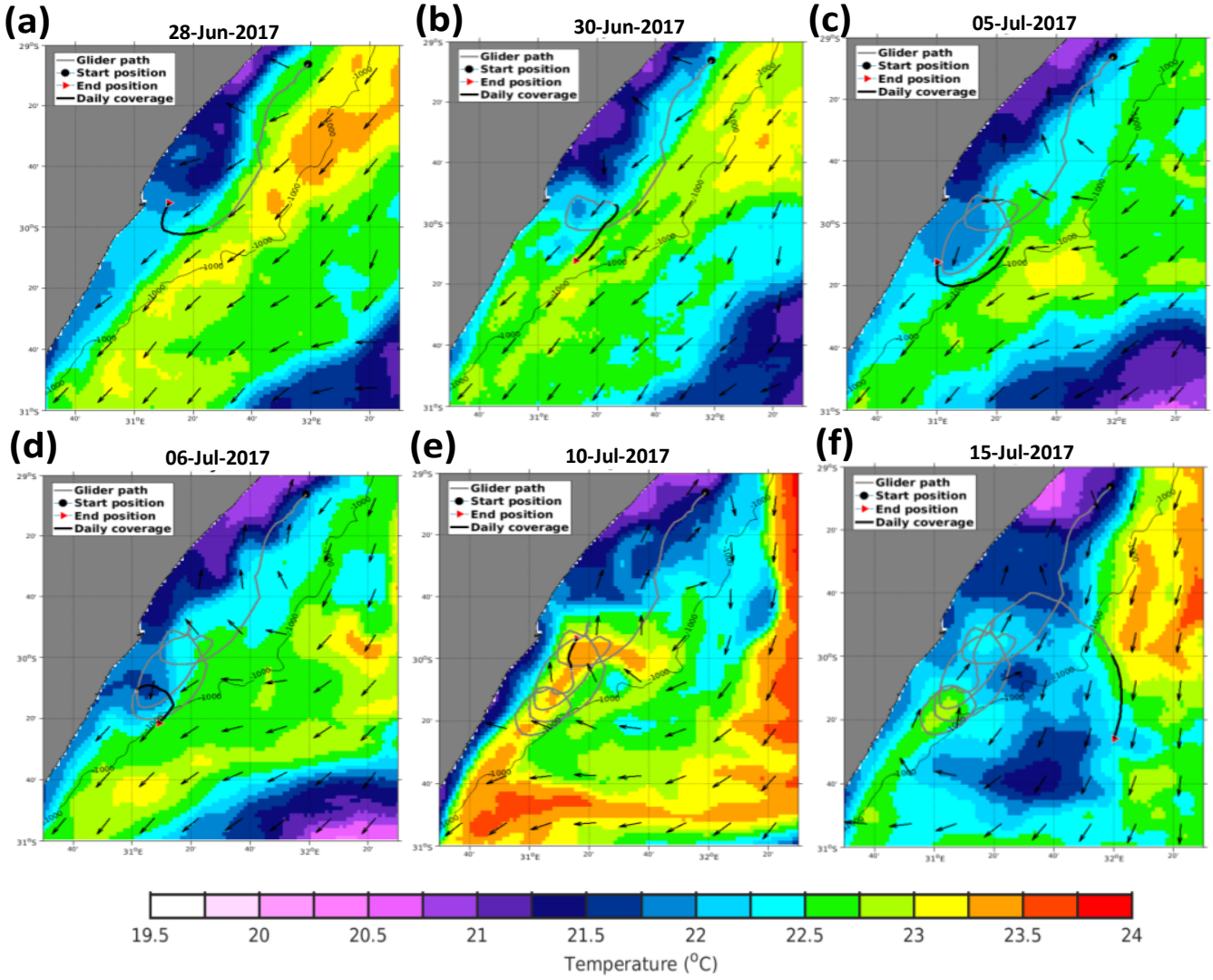

Figure 4.3.1: Sea Surface Temperature maps (a-f) for days June 28th, June 30th, July 5th, July 6th, July 10th and July 15th 2017 respectively. GlobCurrent vectors are normalized by the current speed(the magnitude) and indicated by black arrows. The grey line and black line indicates the path travelled by glider from the start date and the distance covered by glider over a 24-hour period, respectively. The dashed line indicates the 1000 m isobath. Black circle (red triangle) indicate the start (end of glider trajectory on a given date).

Figure 4.3.2 (a) shows the time series of glider and GlobCurrent current speed when the glider was mostly in shallow water in the northern subdomain, and the temperature section plot in Figure 4.3.2 (b) shows the corresponding vertical section of the water temperature along the SG 574 glider path. With the start position located about 25 km inshore of the 1000 m isobath, the glider continues landwards until it reaches 40 km inshore from the 1000 m

isobath. Seaward glider positions closer to the 1000 m isobar correspond to greater current speeds generally exceeding 1 $m.s^{-1}$. These positions are also associated with warmer water temperatures as shown in Figure 4.3.2 (b). Changes in the flow direction at times as the glider moves over the shelf break show that the glider is caught in a small mesoscale eddy identified in Figure 4.3.1 (panels b to e).

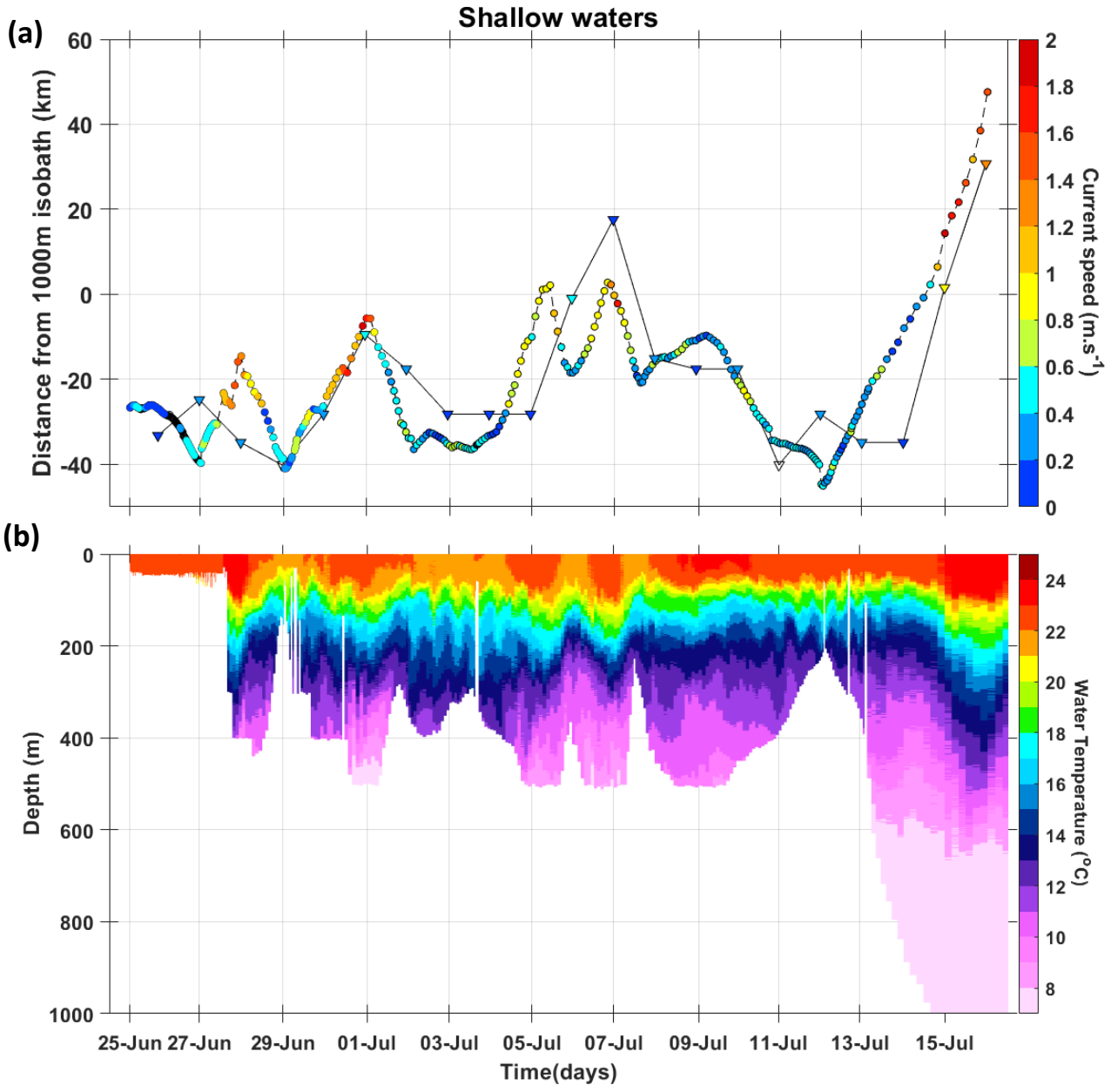

Figure 4.3.2: Time series of (a) current speed from GlobCurrent (triangles) and glider (circles) observations with distance from the 1000 m isobath on the y-axis, and (b) Glider temperature section plot from June 25th to July 16th in shallow waters.

The eddy is estimated to have a diameter of about 40 - 50 km and a 2-day rotational period (figure 4.3.2 b). The rotation period of the cyclonic eddy is comparable to the rotational

period of the Durban Eddy of 2.5 – 3.5 days observed by Guastella and Roberts (2016). Between June 25th and July 11th, the currents in GlobCurrent are weak and directionally uniform in contrast to the glider-observed current velocities which are stronger and much more variable. The limitation of the GlobCurrent product is evident on July 4th and July 8th, where the irregular glider observations capture cyclonic motions around the small eddy while these patterns of rotation are absent in the daily GlobCurrent observations. This is indicative that GlobCurrent simply is unable to capture the small eddy. The presence of a cyclonic eddy can also be noticed from vertical profiles of temperature. The small mesoscale eddy is better captured in the ODYSSEA SST product (Figure 4.3.1 d), with the cold-core of the eddy clearly visible and centered around 30° S;31° E.

4.3.2. Case study of a larger mesoscale feature in deep waters

Larger circulation structures were captured during the 2017 GINA glider mission. The SST maps are presented in figure 4.3.3 for the 4 selected days; July 16th, July 23rd, July 25th and July 29th. The GlobCurrent vectors show the general flow around the glider path and the surrounding waters. Figure 4.3.3 (a) shows the glider trajectory on July 16th as it is caught in a cyclonic eddy with a 21.5 ℃ cold-core. GlobCurrent vectors also show a the cyclonic flow with an inshore flow at 31 °S. The GlobCurrent vectors also show a larger circulation structure centered around 33°S and 31.5° E. North of 31 °S, an inshore northeast flow is shown, flowing in opposition to the main flow direction of the Agulhas Current. This north-easterly flow is associated with warm water, indicative of the inshore edge of the cyclonic eddy associated with the mesoscale meander. The glider makes a small cyclonic turn when closest to the coast. The large mesoscale meander captured by *in-situ* glider observations are characteristic of the well documented Natal Pulse, which is a major driver of variability in the Agulhas Current. After the 16th of July, the glider progresses towards the coast with the leading edge of the meander. As it nears the coast, it undertakes a small cyclonic turn before it gets advected again into another mesoscale cyclonic eddy and continues to move south. On the 23rd of July, the glider once again is caught in a small cyclonic loop when nearing the coast before following a larger cyclonic motion further out at sea. The map on July 25th (figure 4.3.3

c) shows the glider trajectory describing one last cyclonic arc around a large Agulhas Current meander, a Natal Pulse, which is clearly highlighted in the SST imagery. An intense SST contrast cold-core eddy is shown around 34°S and 28°E, with a low SST value of about 17.5 °C.

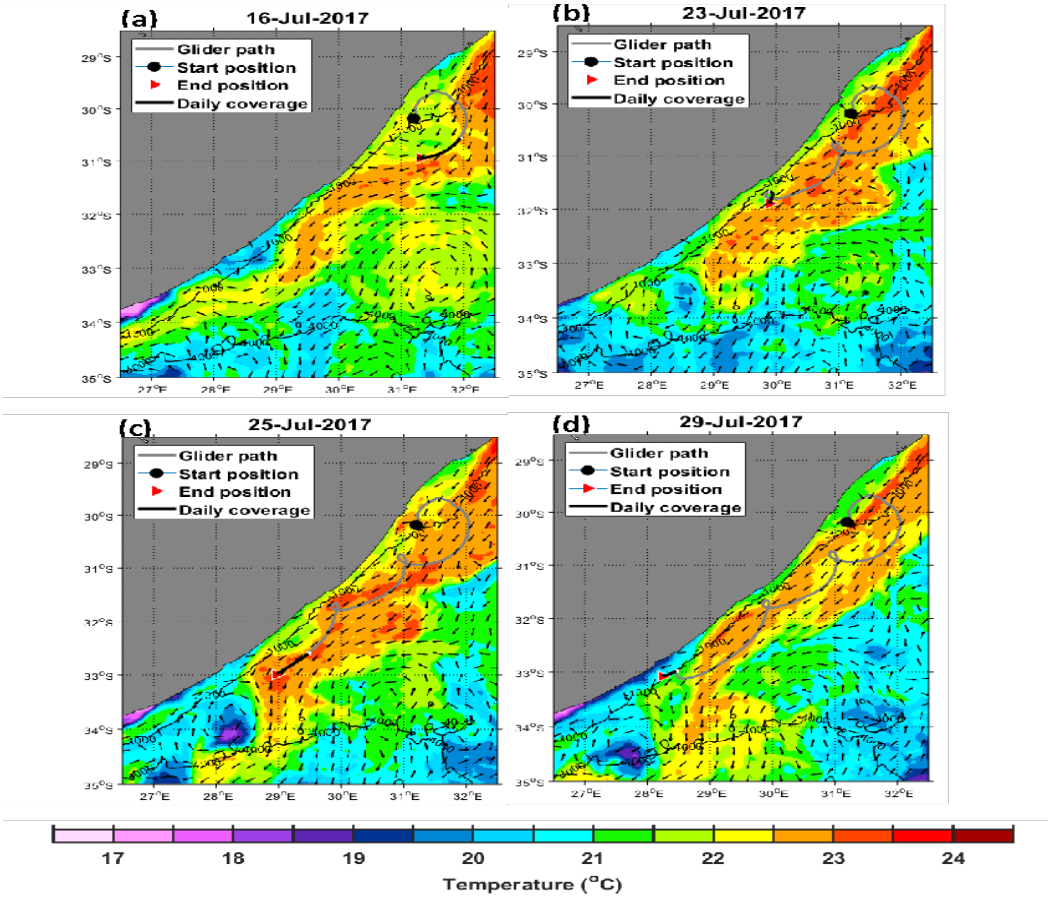

Figure 4.3.3: Sea Surface Temperature maps (a-d) for days July 16th, July 23rd, July 25th and July 29th, respectively. GlobCurrent vectors are normalized by the current speed(the magnitude) and indicated by black arrows. The grey line and black line indicates the path travelled by glider from start date and distance covered by glider over a 24-hour period, respectively. The dashed line indicates the 1000 m isobath. Black circle (red triangle) indicate the start (end) of glider trajectory on a given date.

GlobCurrent vectors indicate a cyclonic flow around this cold center. Both the SST and GlobCurrent data indicate the presence of this large Natal Pulse. This Natal Pulse had resided south of our study area for some time. Past July 29th, the glider is caught into the large Natal Pulse and starts moving offshore. The experiment ended as the glider was being advected offshore in this large Natal Pulse. Between 30°S and 33°S, the glider progresses downstream at an average speed of 27 $km.day^{-1}$, a phase speed that far exceeds the 10 – 20 $km.day^{-1}$

reported for Natal Pulses (Rouault and Penven, 2011). The estimated diameter of the eddy associated with the mesoscale meander ranged between 60 – 100 km and the 30 -50 km offshore excursion. The glider is also never caught into a large cyclonic motion which matches the scale of the mesoscale meanders observed on the SST maps. The trajectory of the glider therefore shows that the glider is caught in a series of meanders or Natal Pulses (a meandering Agulhas Current front) rather than in one single meander. The GlobCurrent flow directions are generally coherent with the glider observations but the glider records greater current speed values.

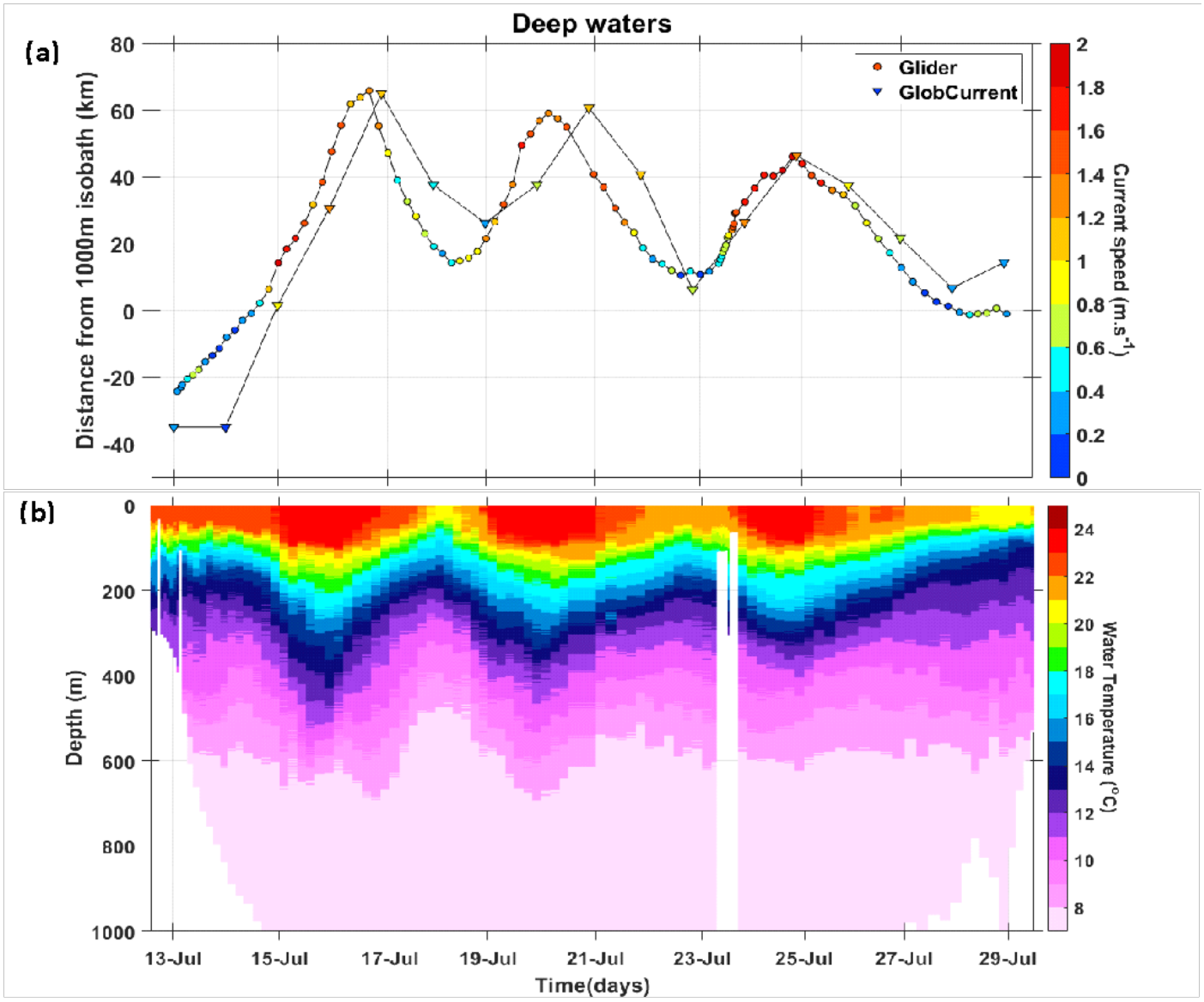

Figure 4.3.4: Time series of (a) current speed from GlobCurrent and glider observations with distance from the 1000 m isobath on the y-axis, and (b) Glider temperature section plot from July 13th to July 29th in deep waters (predominantly > 1000 m).

Figure 4.3.4 (a) shows a time series of current speed as the glider described a meandering path during its southward progression at the Agulhas Current's inshore edge. The time series cover days from July 13th to July 29th with the early days spent in shallow water of about 300m deep before the glider is pulled offshore into a mesoscale eddy-like feature with a width of 60-100 km, based on the SST imagery and the glider trajectory (Figure 4.3.3 and 4.3.4 a). On July 13th, the glider is positioned about 25 km inshore of the 1000 m isobath and the collocated GlobCurrent grid box is over 30 km away from the isobath (Figure 4.3.4 a). With speed values of about 0.4 $m.s^{-1}$ for both the glider and GlobCurrent, the glider moves in the seaward direction towards the 1000 m isobath. Current speed values increase abruptly on July 15th during which the glider position has passed the 1000 m isobath. The glider continues in the seaward direction until it reaches the furthest seaward distance over 60 km from the 1000 m isobath.

At this position, current speed values for the glider and GlobCurrent are exceeding 1.2 $m.s^{-1}$ (Figure 4.3.4 a). A distinctive cyclonic turn is exhibited by the glider along the trajectory from July 15th to July 27th. The trajectory shows the glider moving mostly in the seaward side of the 1000 m isobath. Minimum current speeds of about 0.6 $m.s^{-1}$ are observed when the glider is closer to the 1000 m isobath (Figure 4.3.4 a). In the last loop between July 24th and July 25th, the current speed peaks at a value exceeding 1.6 $m.s^{-1}$. Past July 25th, the speed gradually decreases to a minimum value below 0.2 $m.s^{-1}$ as the glider moves landward. Between July 19th and July 21st, the rapid increase in current speed is not captured by GlobCurrent. GlobCurrent current speeds values are less than 0.4 $m.s^{-1}$ on July 19th while the glider-recorded value exceeds 1.2 $m.s^{-1}$(Figure 4.3.4 a). The depth of the 10 ℃ isotherm gets as deep as about 200m and as shallow as 50m when the glider is far and close to the 1000 m isobath, respectively (Figure 4.3.4 b). The isotherms are at their deepest on July 16th and shallowest on July 18th. Water temperature closest to the surface ranges between 21 ℃ and 24 ℃(Figure 4.3.4 b).

4.4. Other merged satellite products: ODYSSEA SST comparisons

In this section, we present another satellite product that could supplement GlobCurrent for monitoring the Agulhas Current variability. The merged ODYSSEA SST is compared to glider data from all three gliders used in this study. The comparison of merged SST data is broken down by the time, the regions (i.e. subdomains) and water depth i.e. bathymetry below the data points. Figure 4.4.1 shows the time series of SST from the gliders and ODYSSEA datasets, and current vectors from the gliders and GlobCurrent datasets.

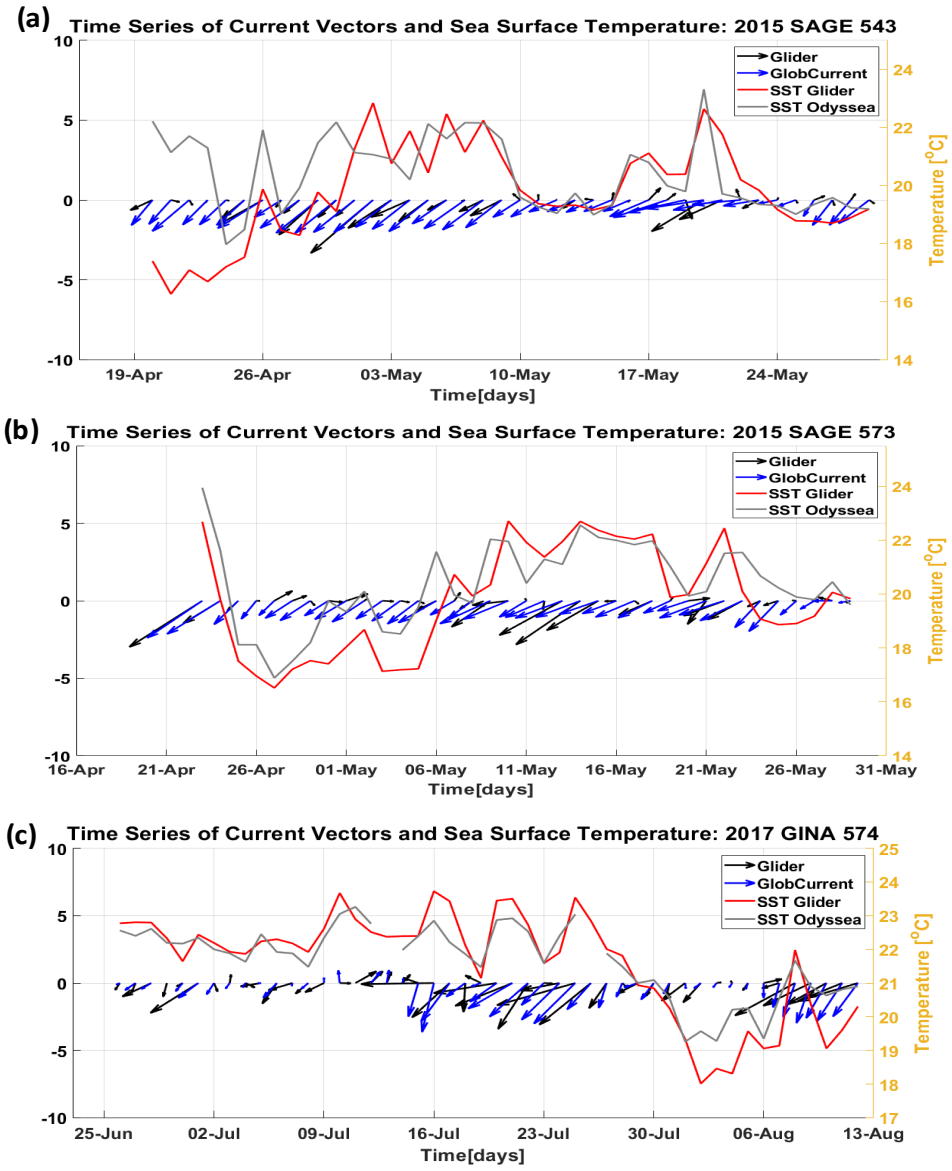

Figure 4.4.1: Time series of daily current vectors extracted from the glider and GlobCurrent datasets. The daily Sea Surface Temperature data from the gliders and ODYSSEA are plotted along with the time series in grey and red lines respectively. Comparisons are made with glider data from (a) SG 543 - SAGE 2015, (b) SG 573 - SAGE 2015 and (b) SG 574 - GINA 2017 gliders. Each current vector and SST dataset is associated with a unique vector colour and line colour respectively as shown in the plots legends.

From May 2nd, the ODYSSEA and glider SST are in relatively good agreement although some of the oscillations in the glider SST between April 30th and May 5th are not well represented in the ODYSSEA SST series (figure 4.4.1. a). The correlation between SSTs from SG 543 and ODYSSEA is statistically significant with a correlation coefficient of 0.36, significant at the 95% confidence level (p-value = 0.021). For SG 573 (figure 4.4.1 b), there is generally a coherence over most of the time series despite higher SST values in the ODYSSEA record between late April and early May 2015. The strength of correlation between the glider and ODYSSEA SSTs is significant with a correlation coefficient of 0.85 (p-value= $2.78\,x\,10^{-11}$). Small discrepancies between glider and ODYSSEA SST are shown on April 26th, between April 29th and May 1st, and on May 12th, with ODYSSEA registering local peaks and drops absent in glider observations. SG 574 generally registered higher SST values than ODYSSEA observations, with a maximum difference of ≈ 1.6 ℃ observed on August 2nd and August 9th. The SG 574 and ODYSSEA SSTs were strongly correlated with a correlation of 0.94; the highest correlation coefficient of the study. The differences between the SG 574 and ODYSSEA SSTs were not statistically significant. Minor discrepancies in local peaks alternating between ODYSSEA and glider observations were observed on June 30th and July 5th.

The summary statistics of the SST observations are shown in table 4.4.1. From the correlation analysis of both current speed and SST, the SST variable exhibited better correspondence between the *in-situ* glider data and satellite ODYSSEA product. Generally, the poor agreement in both current speed and flow direction coincides with local SST minima and shallow water depths suggesting that the product performance is inadequate in the cooler waters which are encountered over the shelf waters and near the coast. Comparisons between the satellite and glider SSTs show that approximately 52% of the paired observations lie below the y=x line indicating that ODYSSEA observations registered higher SST values than the glider-based SSTs (Figure 4.4.2). Data points above the y=x line with SST values typically varying between 19℃ and 24℃ are less spread than those below. The spread SST observation pairs below the y=x line are located in shallower waters (mostly < 500m).

This pattern of distribution suggests that there are more discrepancies in SST observations in shallow water than deeper; which also correspond to coastal or near-shore flows.

Table 4.4.1: Summary statistics of all the time-series Sea Surface Temperature data from the in-situ *glider and satellite ODYSSEA. The 2nd – 5th columns show the minimum, maximum, mean and standard deviation of each glider and corresponding ODYSSEA observations. From the 6th to the 10th column, the mean bias, percentage difference, percentage RMSE , correlation and the p-value for the correlation are calculated from ODYSSEA-glider pairs at corresponding times, locations and subdomains. Northern sub., Middle sub. and Southern Sub. represent the (a) Northern < 32°S, (b) Middle 34 > & > 32°S and (c) Southern > 34°S subdomains.*

Data Source	Min (°C)	Max (°C)	Mean (°C)	Standard deviation (°C)	Mean bias (°C)	% Difference	% RMSE	Correlation (r)	p-value (corr)
SG 543	16,26	22,84	19,71	1,65	0,67	3,41	78,08	0,36	0,021
ODYSSEA(543)	17,97	23,31	20,39	1,29					
SG 573	16,52	22,7	19,8	1,97	0,56	2,81	78,86	0,85	2,78E-11
ODYSSEA(573)	16,89	23,94	20,36	1,55					
SG 574	18,01	23,73	21,61	1,54	0,05	0,24	67,44	0,94	6,69E-23
ODYSSEA(574)	19,26	23,26	21,66	1,06					
Northern sub. (Glider)	21,15	23,73	22,48	0,62	-0,21	-0,94	75,51	0,78	6,33E-06
Northern sub. (ODYSSEA)	21,47	23,26	22,27	0,48					
Middle sub. (Glider)	18,01	23,54	20,68	1,72	0,32	1,56	65,44	0,93	5,86E-10
Middle sub. (ODYSSEA)	19,26	23,04	21	1,15					
Southern sub. (Glider)	16,26	22,84	19,76	1,8	0,62	3,12	78,5	0,64	3,68E-10
Southern sub. (ODYSSEA)	16,89	23,94	20,37	1,41					
All Gliders	16,26	23,73	20,47	1,92	0,39	1,89	73,82	0,78	3,17E-26
All ODYSSEA	16,89	23,94	20,85	1,43					

Figure 4.4.3 shows the SST comparisons for all 3 subdomains. The northern subdomain had mean SST values of 22.48℃ (s= 0.62℃)and 22.27℃(s= 0.48℃) from glider and ODYSSEA respectively (Figure 4.4.3 a). With a statistically significant correlation (r= 0.78; p-value=$6.33\ x\ 10^{-6}$), glider records in this subdomain had, on average, lower SST values than the ODYSSEA with a percentage difference of less than 1%. The SST values for the northern subdomain also have a lower spread than the other two subdomains. The middle subdomain had the highest significant correlation (r= 0.93; p-value=$5.86\ x\ 10^{-10}$) between the glider and the ODYSSEA observations with mean values of 20.68℃(s= 1.72℃) and 21℃(s= 1.15℃) respectively (Figure 4.4.3 b). The southern subdomain exhibited the highest mean bias (0.62℃; approximately 3.12% difference) and also registered the lowest minimum SST values (Figure 4.4.3 c).

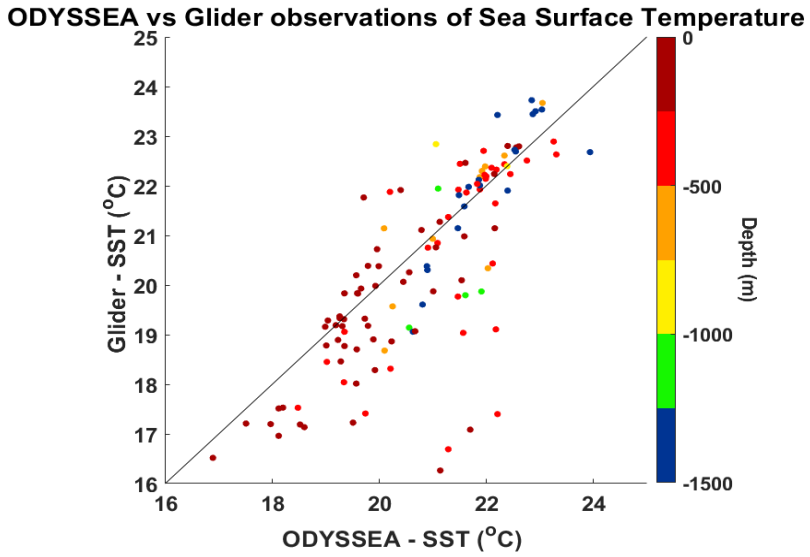

Figure 4.4.2: Scatter plot of daily ODYSSEA vs Glider observations of Sea Surface Temperature (SST) with the colours representing the maximum water depth on that day (from GEBCO bathymetry). The diagonal line represents the line y = x.

The ODYSSEA record registered a higher mean value (mean=20.37℃ ; s=1.41℃) than the glider record (mean= 19.76℃;s=1.8℃). However, the correlation between the glider and ODYSSEA records was statistically significant (r= 0.64; p-value= $3.68\ x\ 10^{-10}$). The combined glider data ("All glider") and ODYSSEA records ("All ODYSSEA") had a significant correlation (r= 0.78; p-value= $3.17\ x\ 10^{-26}$) with a mean bias of 0.39℃.

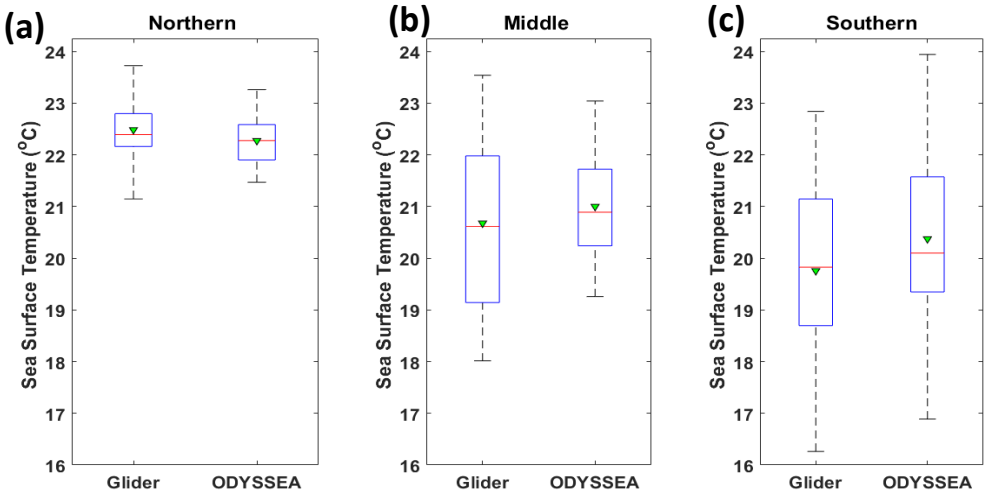

Figure 4.4.3: Boxplot of Sea Surface Temperature observations from the glider data and ODYSSEA merged SSTS for the (a) Northern < 32°S, (b) Middle 34 > & > 32°S and (c) Southern > 34°S subdomains. The red line and green triangle mark the median and mean values respectively. The blue box represents the interquartile range; lower quartile (Q1) at the bottom and upper quartile (Q3) at the top. The dashed lines represent data points outside the interquartile range up to the maximum and minimum values at the tips.

In this chapter, daily averages of glider current speeds were compared to the Total 15m, geostrophic and Ekman 15m GlobCurrent time series. Significant correlations were found between the glider observations and the GlobCurrent current speeds although a poorer agreement was found in the direction of the current flow. The Ekman 15m current had no significant relations with the glider observations and exhibited very little variability with maximum speeds barely exceeding 0.1 $m.s^{-1}$. Significant differences in the mean values between the glider and GlobCurrent were found in the northern and southern subdomain; the middle subdomain had no significant differences. The GlobCurrent mean current speed in the northern (southern) domain was found to be lower (greater) than the mean speed of other subdomains. GlobCurrent overestimated measurements in the shallow waters, mostly in less than 250m water depths and overestimated measurement in deeper waters i.e. mostly points between 500m and 750m water depths, and points over 1250m water depth. Using all the glider data collocated temporally and spatially with the GlobCurrent satellite observations, we found that GlobCurrent has directional errors in addition to current speed magnitude. The glider observations showed a northeast-southwest major axis of the current flow with high strong south-westwards flows in deeper waters (> 750m depth). In contrast, GlobCurrent exhibited clustered U and V observations without north-east flows in shallow waters in contrast to the glider observations. There was a good representation of the general Agulhas Current flow and large mesoscale features by GlobCurrent, mainly in deep waters. However, GlobCurrent presented poor coherence for the representation for current flows in shallow waters, small mesoscale and submesoscale features. The poor performance of GlobCurrent is exhibited particularly when the collocated glider captured the Durban Eddy in the northern subdomain. ODYSSEA SST field provided a good complement in imaging small mesoscale features where GlobCurrent lacked the ability to resolve the signals. The ODYSSEA SSTs also presented the best correlation strength with glider data than GlobCurrent, further supporting its applicability to capturing variability in the inshore edge of the Agulhas Current.

CHAPTER 5: DISCUSSION

The glider datasets generally exhibited more variability in current speed than the relatively steady GlobCurrent product with smaller oscillations from low to high speeds over timescales of days, in direct contrast to the findings of Cancet et al. (2019) where in-situ observations were steadier and satellites observations were more variable. The low current speed variability around mean values is further corroborated by the %RMSE values. Looking at the U vs V comparisons by depth, we observed discrepancies in current flow components (Figure 4.1.3). GlobCurrent showed more clustered observations with the meridional component dominating deeper (> 750m) flow while the zonal component dominated shallow waters (Figure 4.1.3 a). From the GlobCurrent observations, there is no exhibition of the major flow axis. Glider observations (figure 4.1.3 b), on the contrary, exhibit a more diagonal spread along the y=x line indicating a northeast-southwest major axis of current flow. There are notable observations of north-eastward flows in the glider record that are not represented in the GlobCurrent records. The correlation between glider-based observations and GlobCurrent observations were best when computed using the current speed magnitude rather than when comparing zonal and meridional velocities. This indicates that GlobCurrent has directional errors in addition to the magnitude of the current speed. Cancet et al. (2019) and Hart-Davis et al. (2018) similarly noted that current directions were poorly represented in the GlobCurrent product even though the GlobCurrent dataset correctly identified the mean flow magnitude.

The current speed observations from GlobCurrent product are mainly based on the merged altimetry product produced by Ssalto/Duacs and therefore suffer from the same limitation. The limitations of the merged Ssalto/Duacs altimetry products are due to include 1) close proximity to the coast, 2) the low effective temporal and spatial resolution of the altimetry products and 3) the fact that the current flow derived is geostrophic and not absolute (e.g. Rio et al., 2014; Ubelmann et al., 2015). In the northern subdomain, for example, GlobCurrent was unable to capture the current flow associated with the Durban Eddy. The Durban Eddy

had an ellipsoidal shape with a size of (30-50 km), smaller than the Durban eddies presented in previous studies but still within the mesoscale range size (Roberts et al., 2010; Guastella and Roberts, 2016). The time spent by the glider in cyclonic motions around the eddy (over 10 days) exceeds the average lifespan (8.6 days) previously reported for a Durban Eddy although it remains within the maximum lifespan of 19 days (Guastella and Roberts 2016). This observed period suggests that the Durban Eddy was in a maturation phase as its core became increasingly colder. Despite its mesoscale size and longevity, GlobCurrent failed to capture the presence of this Durban Eddy. The poor performance of GlobCurrent in this region can be attributed to the proximity of the Agulhas Current to the coast and the rapid evolution of the Durban Eddy feature. The cross-shelf dynamics in the northern subdomain are known to exhibit high variability dominated by frequent inshore current reversal associated with the Durban Eddy and occasional progression of Natal Pulses (Guastella and Roberts, 2016). The poor match between the GlobCurrent and glider current speeds and position is a clear example of how temporal and spatial bias can alias small mesoscale features such as the Durban Eddy (Figure 4.3.2 d). The Durban Eddy is a distinctive feature of the local circulation in the Natal bight region and it occurs on a semi-permanent basis (Guastella and Roberts 2016). The inability of the GlobCurrent product to capture these features implies that the local circulation of the southern Natal Bight cannot adequately be resolved in the GlobCurrent product. GlobCurrent was also not able to capture the submesoscale features observed by the gliders during SAGE in the southern subdomain; the Agulhas Bank region. GlobCurrent generally overestimated the current speeds in the southern subdomain although the flow direction closer to the 1000 m isobath was well represented. For small-sized features and flows near strong fronts, GlobCurrent fails to resolve the current flow. Other studies have also noted that the merging and interpolation techniques used in the generation of current estimates from multiple altimeters contribute to the poor performance of the GlobCurrent product (e.g. Meyer et al., 2017). The insufficient temporal and spatial resolution leads to an inadequate representation of small mesoscale features and other dynamics with temporal scales over a few days (Hart-Davis et al., 2018). Our observations of GlobCurrent discrepancies are in support of other studies that cautioned the use of GlobCurrent products for application in narrow shelves and shallow waters noting

that the product still requires improvement for coastal water application (e.g. Cancet et al., 2019). For both the northern and southern subdomains, the current flows captured by the glider were associated with small mesoscale to submesoscale features and region of strong fronts that GlobCurrent failed to resolve.

Aside from the limitation on representing small scale features and flows near coastal regions, GlobCurrent performed well in representing the overall flow of the Agulhas Current and other large mesoscale features in agreement with previous studies (e.g. Beal et al., 2015). A generally good agreement in current flow direction between the GlobCurrent and glider datasets was exhibited in the middle subdomain at a time when mesoscales meanders were observed along the Agulhas Current's inshore front. The rapid progression of the glider downstream during that time (at a rate of $27 km.day^{-1}$) shows that the glider was not in a Natal Pulse but rather was travelling with a train of meanders. Rouault and Penven (2011) remarked on the complex evolution and dynamics of mesoscale meanders like Natal pulse and observed that these structures were not always solitary meanders but instead were often associated with several meanders propagating together southward. GlobCurrent streamlines exhibited a consistent agreement with the flow direction of the glider including the cyclonic loops around the mesoscale meander. Two large Natal Pulses, observed in the Natal Bight region and offshore Port Elizabeth were also well captured in the GlobCurrent product. The large mesoscale meander feature in our study between July 14th and July 29th clearly dominated the recirculation of waters in the bight and downstream along the coast. The reliability of GlobCurrent's representation of surface current flow in deeper waters (>1000 m) has also been reported by other studies (e.g. Cancet et al., 2019). Our findings support the reliability of GlobCurrent to represent large mesoscale features and current flow in deep waters.

The high-resolution, merged, ODYSSEA SST product demonstrated a good ability to capture SST variation even at the finer scales sampled by the glider. The *in-situ* temperatures and the satellite SST records were more strongly correlated than the gliders and GlobCurrent current

speeds. The general Agulhas Current flow was well represented indicating the frontal region with steep SST gradients marking the inshore boundary of the Agulhas Current and an adequate representation of the meandering current flow. In our study. The use of the SST fields to complement GlobCurrent proved useful, particularly in imaging small mesoscale features in the northern subdomain i.e. Durban Eddy. Previous studies have successfully used SST fields and altimetry observations to identify and characterize ocean feature and circulation patterns (e.g. Roberts and Nieuwenhuys, 2016; Jury, 2015, Krug and Tournadre, 2012, Rouault and Penven, 2011, Isern-Fontanet et al., 2006). The realized value of exploiting satellite SST fields to improve surface current measurements has led to the recent development of a new experimental product, the Ssalto/Duacs experimental products which combines altimetry and SST (e.g. Rio and Santoleri, 2018).

CHAPTER 6: SUMMARY AND CONCLUSIONS

In this study, *in-situ* data from glider observations from the 2015 SAGE and 2017 GINA programs, and satellite observations from the GlobCurrent products and the ODYSSEA SST fields were analysed and compared. Our overarching goal was to evaluate the ability of the GlobCurrent product to track and resolve the Agulhas Current's cross-shelf dynamics. More specifically, the study (i) evaluated the accuracy of GlobCurrent product over the Agulhas current region; (ii) assessed the ability of GlobCurrent product to represent Agulhas Current's inshore frontal mesoscale processes; (iii) explored the complementary use of merged satellite SST products to better track and monitor the front variability of the Agulhas Current over the continental shelf. Based on the comparison and correlation analysis of the GlobCurrent product against the in-situ glider data, it can be concluded that GlobCurrent provides accurate observations of the Agulhas Current flow in deep waters although the product is severely challenged is shallower coastal waters. The results also show that GlobCurrent performs poorly when fast-evolving and small mesoscale features occur. The GlobCurrent product was also not able to adequately capture a small mesoscale feature: the Durban Eddy in the KZN bight region. This research study clearly illustrates the limitation of the GlobCurrent product for studying current variability in shelf waters, coastal waters and regions dominated by small mesoscale variability. GlobCurrent observations often have directional errors in addition to the current speed inaccuracies. While the limitation of the altimetry-based product for capturing small mesoscale and fast-evolving features is demonstrated, this study also provides new insights on the use of other merged satellite products i.e. merged ODYSSEA SSTs, which may compensate for the GlobCurrent product shortfalls.

From the presented conclusions, caution must be exercised when interpreting altimetry-based satellite observations in shallow flows close to the coast and small mesoscale features, considering the limited performance of altimetry satellite products close to the coast and the effective resolution of merged products. It also recommended that researchers complement altimetry-based satellite products like GlobCurrent with other merged satellite observation

products, e.g. ODYSSEA SST, for better imaging of small mesoscale processes and features in shallow waters like the KZN bight region (e.g. Rio et al., 2016, 2018). More work is required to improve the methods and tools to capture mesoscale processes in the Agulhas Current region adequately. The high-resolution glider data has proved to be an important complementary validation of satellite products. Systematic exploration of multi-satellite sensor synergy combined with *in-situ* data and model fields is therefore also expected to improve and provide better abilities to monitor mesoscale features and upper ocean dynamics (Johannessen et al., 2016).

BIBLIOGRAPHY:

- Backeberg, B.C., Johannessen, J.A., Bertino, L. and Reason, C.J., 2008. The greater Agulhas Current system: An integrated study of its mesoscale variability. Journal of Operational Oceanography, 1(1), pp.29-44.
- Beal, L.M. and Bryden, H.L., 1999. The velocity and vorticity structure of the Agulhas Current at 32 S. Journal of Geophysical Research: Oceans, 104(C3), pp.5151-5176.
- Beal, L.M. and Elipot, S., 2016. Broadening not strengthening of the Agulhas Current since the early 1990s. Nature, 540(7634), p.570.
- Beal, L.M., Elipot, S., Houk, A. and Leber, G.M., 2015. Capturing the transport variability of a western boundary jet: Results from the Agulhas Current Time-Series Experiment (ACT). Journal of Physical Oceanography, 45(5), pp.1302-1324.
- Biastoch, A., Böning, C.W. and Lutjeharms, J.R.E., 2008a. Agulhas leakage dynamics affects decadal variability in Atlantic overturning circulation. Nature, 456(7221), p.489.
- Biastoch, A., Lutjeharms, J.R.E., Böning, C.W. and Scheinert, M., 2008b. Mesoscale perturbations control inter-ocean exchange south of Africa. Geophysical Research Letters, 35(20).
- Boyd, F.A., 1994. Physical forcing and circulation patterns on the Agulhas Bank. South African Journal of Science, 90(3), pp.143-154.
- Braby, L., Backeberg, B.C., Ansorge, I., Roberts, M.J., Krug, M. and Reason, C.J., 2016. Observed eddy dissipation in the Agulhas Current. Geophysical Research Letters, 43(15), pp.8143-8150.
- Bryden, H.L., Beal, L.M. and Duncan, L.M., 2005. Structure and transport of the Agulhas Current and its temporal variability. Journal of Oceanography, 61(3), pp.479-492.
- Campos, E.J., Velhote, D. and da Silveira, I.C., 2000. Shelf break upwelling driven by Brazil Current cyclonic meanders. Geophysical Research Letters, 27(6), pp.751-754.
- Cancet, M., Griffin, D., Cahill, M., Chapron, B., Johannessen, J. and Donlon, C., 2019. Evaluation of GlobCurrent surface ocean current products: A case study in Australia. Remote sensing of environment, 220, pp.71-93.

- de Ruijter, W.P., Van Leeuwen, P.J. and Lutjeharms, J.R., 1999. Generation and evolution of Natal Pulses: solitary meanders in the Agulhas Current. Journal of physical oceanography, 29(12), pp.3043-3055.
- Duncombe Rae, C.M., 1991. Agulhas retroflection rings in the South Atlantic Ocean: an overview. South African Journal of Marine Science, 11(1), pp.327-344.
- Elipot, S. and Beal, L.M., 2015. Characteristics, energetics, and origins of Agulhas Current meanders and their limited influence on ring shedding. Journal of Physical Oceanography, 45(9), pp.2294-2314.
- Eriksen, C.C., Osse, T.J., Light, R.D., Wen, T., Lehman, T.W., Sabin, P.L., Ballard, J.W. and Chiodi, A.M., 2001. Seaglider: A long-range autonomous underwater vehicle for oceanographic research. IEEE Journal of oceanic Engineering, 26(4), pp.424-436.
- Ferrari, R. and Wunsch, C., 2009. Ocean circulation kinetic energy: Reservoirs, sources, and sinks. Annual Review of Fluid Mechanics, 41.
- Garzoli, S.L., Gordon, A.L., Kamenkovich, V., Pillsbury, D. and Duncombe-Rae, C., 1996. Variability and sources of the southeastern Atlantic circulation. Journal of Marine Research, 54(6), pp.1039-1071.
- Gründlingh, M.L., 1983. On the course of the Agulhas Current. South African Geographical Journal, 65(1), pp.49-57.
- Guastella, L.A. and Roberts, M.J., 2016. Dynamics and role of the Durban cyclonic eddy in the KwaZulu-Natal Bight ecosystem. African Journal of Marine Science, 38(sup1), pp.S23-S42.
- Gula, J., Molemaker, M.J. and McWilliams, J.C., 2015. Topographic vorticity generation, submesoscale instability and vortex street formation in the Gulf Stream. Geophysical Research Letters, 42(10), pp.4054-4062.
- Gula, J., Molemaker, M.J. and McWilliams, J.C., 2016. Topographic generation of submesoscale centrifugal instability and energy dissipation. Nature communications, 7, p.12811.
- Halo, I., Penven, P., Backeberg, B., Ansorge, I., Shillington, F. and Roman, R., 2014. Mesoscale eddy variability in the southern extension of the East Madagascar Current:

Seasonal cycle, energy conversion terms, and eddy mean properties. Journal of Geophysical Research: Oceans, 119(10), pp.7324-7356.

- Hart-Davis, M.G., Backeberg, B.C., Halo, I., van Sebille, E. and Johannessen, J.A., 2018. Assessing the accuracy of satellite derived ocean currents by comparing observed and virtual buoys in the Greater Agulhas Region. Remote Sensing of Environment.
- IFREMER/CERSAT. 2007. GHRSST Level 4 ODYSSEA Global Foundation Sea Surface Temperature Analysis. Ver. 1.0. PO.DAAC, CA, USA. Dataset accessed [2018-07-13] at http://dx.doi.org/10.5067/GHGOY-4FE01.
- Isern-Fontanet, J., Chapron, B., Lapeyre, G. and Klein, P., 2006. Potential use of microwave sea surface temperatures for the estimation of ocean currents. Geophysical research letters, 33(24).
- Johannessen, J.A., Chapron, B., Collard, F., Rio, M.H., Piollé, J.F., Gaultier, L., Quartly, G., Shutler, J., Raj, R., Donlon, C. and Danielson, R., 2016, September. GlobCurrent: Multisensor synergy for surface current estimation. ESA.
- Jury, M.R., 2015. Passive suppression of South African rainfall by the Agulhas Current. Earth Interactions, 19(13), pp.1-14.
- Klein, M.L. and Shinoda, W., 2008. Large-scale molecular dynamics simulations of self-assembling systems. Science, 321(5890), pp.798-800.
- Krug, M. and Tournadre, J., 2012. Satellite observations of an annual cycle in the Agulhas Current. Geophysical Research Letters, 39(15).
- Krug, M., Swart, S. and Gula, J., 2017. Submesoscale cyclones in the Agulhas current. Geophysical Research Letters, 44(1), pp.346-354.
- Krug, M., Tournadre, J. and Dufois, F., 2014. Interactions between the Agulhas Current and the eastern margin of the Agulhas Bank. Continental Shelf Research, 81, pp.67-79.
- Krug, M.J., Swart, S. and Hermes, J., 2018. Ocean gliders ride the research wave in the Agulhas Current.
- Leber, G.M. and Beal, L.M., 2014. Evidence that Agulhas Current transport is maintained during a meander. Journal of Geophysical Research: Oceans, 119(6), pp.3806-3817.

- Leber, G.M., Beal, L.M. and Elipot, S., 2017. Wind and current forcing combine to drive strong upwelling in the Agulhas Current. Journal of Physical Oceanography, 47(1), pp.123-134.
- Lutjeharms, J.R., 2006. The coastal oceans of south-eastern Africa (15, W). The sea, 14, pp.783-834.
- Lutjeharms, J.R., Boebel, O., van der Vaart, P.C., de Ruijter, W.P., Rossby, T. and Bryden, H.L., 2001. Evidence that the Natal Pulse involves the Agulhas Current to its full depth. Geophysical research letters, 28(18), pp.3449-3452.
- Lutjeharms, J.R.E. and Van Ballegooyen, R.C., 1988. The retroflection of the Agulhas Current. Journal of Physical Oceanography, 18(11), pp.1570-1583.
- Lutjeharms, J.R.E., Boebel, O. and Rossby, H.T., 2003. Agulhas cyclones. Deep Sea Research Part II: Topical Studies in Oceanography, 50(1), pp.13-34.
- Mantovanelli, A., Keating, S., Wyatt, L.R., Roughan, M. and Schaeffer, A., 2017. Lagrangian and Eulerian characterization of two counter-rotating submesoscale eddies in a western boundary current. Journal of Geophysical Research: Oceans, 122(6), pp.4902-4921.
- Martin, M., Dash, P., Ignatov, A., Banzon, V., Beggs, H., Brasnett, B., Cayula, J.F., Cummings, J., Donlon, C., Gentemann, C. and Grumbine, R., 2012. Group for High Resolution Sea Surface temperature (GHRSST) analysis fields inter-comparisons. Part 1: A GHRSST multi-product ensemble (GMPE). Deep Sea Research Part II: Topical Studies in Oceanography, 77, pp.21-30.
- McWilliams, J.C., 2016. Submesoscale currents in the ocean, P. Roy. Soc. A, 472, 20160117.
- Meyer, I., Braby, L., Krug, M. and Backeberg, B., 2017. Mapping the ocean current strength and persistence in the Agulhas to inform marine energy development. In Marine Renewable Energy (pp. 179-215). Springer, Cham.
- Okkonen, S.R., Weingartner, T.J., Danielson, S.L., Musgrave, D.L. and Schmidt, G.M., 2003. Satellite and hydrographic observations of eddy-induced shelf-slope exchange in the northwestern Gulf of Alaska. Journal of Geophysical Research: Oceans, 108(C2).
- Pearce, A.F., 1977. The shelf circulation off the east coast of South Africa.

- Pivan, X., Krug, M. and Herbette, S., 2016. Observations of the vertical and temporal evolution of a Natal Pulse along the Eastern Agulhas Bank. Journal of Geophysical Research: Oceans, 121(9), pp.7108-7122.
- Rio, M.H. and Santoleri, R., 2018. Improved global surface currents from the merging of altimetry and Sea Surface Temperature data. Remote Sensing of Environment.
- Rio, M.H., Mulet, S. and Picot, N., 2014. Beyond GOCE for the ocean circulation estimate: Synergetic use of altimetry, gravimetry, and in situ data provides new insight into geostrophic and Ekman currents. Geophysical Research Letters, 41(24), pp.8918-8925.
- Rio, M.H., Santoleri, R., Bourdalle-Badie, R., Griffa, A., Piterbarg, L. and Taburet, G., 2016. Improving the altimeter-derived surface currents using high-resolution sea surface temperature data: A feasibility study based on model outputs. Journal of Atmospheric and Oceanic Technology, 33(12), pp.2769-2784.
- Rio, M.H., Schaeffer, P., Hernandez, F. and Lemoine, J.M., 2005, April. The estimation of the ocean Mean Dynamic Topography through the combination of altimetric data, in-situ measurements and GRACE geoid: From global to regional studies. In Proceedings of the GOCINA international workshop, Luxembourg.
- Roberts, M.J. and Nieuwenhuys, C., 2016. Observations and mechanisms of upwelling in the northern KwaZulu-Natal Bight, South Africa. African Journal of Marine Science, 38(sup1), pp.S43-S63.
- Roberts, M.J., Nieuwenhuys, C. and Guastella, L.A., 2016. Circulation of shelf waters in the KwaZulu-Natal Bight, South Africa. African Journal of Marine Science, 38(sup1), pp.S7-S21.
- Roberts, M.J., Van der Lingen, C.D., Whittle, C. and Van den Berg, M., 2010. Shelf currents, lee-trapped and transient eddies on the inshore boundary of the Agulhas Current, South Africa: their relevance to the KwaZulu-Natal sardine run. African Journal of Marine Science, 32(2), pp.423-447.
- Rouault, M.J. and Penven, P., 2011. New perspectives on Natal Pulses from satellite observations. Journal of Geophysical Research: Oceans, 116(C7).

- Roughan, M., Keating, S.R., Schaeffer, A., Cetina Heredia, P., Rocha, C., Griffin, D., Robertson, R. and Suthers, I.M., 2017. A tale of two eddies: The biophysical characteristics of two contrasting cyclonic eddies in the East Australian Current System. Journal of Geophysical Research: Oceans, 122(3), pp.2494-2518.
- Roughan, M., Macdonald, H.S., Baird, M.E. and Glasby, T.M., 2011. Modelling coastal connectivity in a Western Boundary Current: Seasonal and inter-annual variability. Deep Sea Research Part II: Topical Studies in Oceanography, 58(5), pp.628-644.
- Rudnick, D.L., Gopalakrishnan, G. and Cornuelle, B.D., 2015. Cyclonic eddies in the Gulf of Mexico: Observations by underwater gliders and simulations by numerical model. Journal of Physical Oceanography, 45(1), pp.313-326.
- Rusello, P.J., Yahnker, C. and Morris, M., 2012, October. Improving depth averaged velocity measurements from seaglider with an advanced acoustic current profiler, the nortek ad2cp-glider. In 2012 Oceans (pp. 1-8). IEEE.
- Schaeffer, A. and Roughan, M., 2015. Influence of a western boundary current on shelf dynamics and upwelling from repeat glider deployments. Geophysical Research Letters, 42(1), pp.121-128.
- Schouten, M.W., De Ruijter, W.P. and Van Leeuwen, P.J., 2002. Upstream control of Agulhas Ring shedding. Journal of Geophysical Research: Oceans, 107(C8), pp.23-1.
- Stommel, H., 1948. The westward intensification of wind-driven ocean currents. Eos, Transactions American Geophysical Union, 29(2), pp.202-206.
- Stramma, L. and Lutjeharms, J.R., 1997. The flow field of the subtropical gyre of the South Indian Ocean. Journal of Geophysical Research: Oceans, 102(C3), pp.5513-5530.
- Tsugawa, M. and Hasumi, H., 2010. Generation and growth mechanism of the Natal Pulse. Journal of Physical Oceanography, 40(7), pp.1597-1612.
- Ubelmann, C., Klein, P. and Fu, L.L., 2015. Dynamic interpolation of sea surface height and potential applications for future high-resolution altimetry mapping. Journal of Atmospheric and Oceanic Technology, 32(1), pp.177-184.

- van Leeuwen, P.J., de Ruijter, W.P. and Lutjeharms, J.R., 2000. Natal pulses and the formation of Agulhas rings. Journal of Geophysical Research: Oceans, 105(C3), pp.6425-6436.
- Zhai, X., Johnson, H.L. and Marshall, D.P., 2010. Significant sink of ocean-eddy energy near western boundaries. Nature Geoscience, 3(9), p.608.